Evidence of deep and bottom water formation in the western Weddell Sea

Oliver Huhn[a,1], Hartmut H. Hellmer[b], Monika Rhein[a], Wolfgang Roether[a], Christian Rodehacke[a,c], Michael P. Schodlok[b,d], Michael Schröder[b]

[a] Institut für Umweltphysik, Universität Bremen, Bremen, Germany

[b] Alfred-Wegener-Institut, Bremerhaven, Germany

[c] now at Zentrum für Marine und Atmosphärische Wissenschaften, Hamburg, Germany

[d] now at Jet Propulsion Laboratory, California Institute of Technology, Pasadena, CA, USA

Abstract

During Ice Station POLarstern (ISPOL, RV Polarstern cruise ANT XXII/2, Nov. 2004 to Jan. 2005) hydrographic and tracer observations were obtained in the western Weddell Sea while drifting closely in front of the Larsen Ice Shelf. These observations indicate recently formed Weddell Sea Bottom Water, which contains significant contributions of glacial melt water in its upper part, and High Salinity Shelf Water in its lower layer. The formation of this bottom water cannot be related to the known sources in the south, the Filchner-Ronne Ice Shelf. We show that this bottom water is formed in the western Weddell Sea, most likely in interaction with the Larsen C Ice Shelf. By applying an Optimum Multiparameter Analysis (OMP) using temperature, salinity, and noble gas observations (helium isotopes and neon), we obtained mean glacial melt water fractions of about 0.1% in the bottom water. On sections across the Weddell Gyre further north melt water fractions are still in the order of 0.04%. Using chlorofluorocarbons (CFCs) as age tracers, we deduced a mean transit time between the western source and the bottom water found on the slope toward the north (9 ± 3 years). This transit time is larger and the inferred transport rate is small in comparison to previous findings. But accounting for a loss of the initially formed bottom water volume due to mixing and renewal of Weddell Sea Deep Water, a formation rate of 1.1 ± 0.5 Sv in the western Weddell Sea is

[1] Corresponding author:
Institut für Umweltphysik (IUP), Abt. Ozeanographie, Universität Bremen, D-28359 Bremen, Germany
Phone +49-421-218 4567, Fax +49-421-218 7018,
E-mail: ohuhn@physik.uni-bremen.de

plausible. This implies a basal melt rate of 35 ± 19 Gt/year or 0.35 ± 0.19 m/year at the Larsen Ice Shelf. This bottom water is shallow enough that it could leave the Weddell Basin through the gaps in the South Scotia Ridge to supply Antarctic Bottom Water. These findings emphasize the role of the western Weddell Sea in deep and bottom water formation, particularly in view of changing environmental conditions due to climate variability, which might induce enhanced melting or even decay of ice shelves.

Keywords: Weddell Sea, Larsen Ice Shelf, Weddell Sea Bottom Water (WSBW) formation, Ice Shelf Water (ISW), glacial melt water, tracer, helium, neon, CFC

1. Introduction

Antarctic Bottom Water (AABW) is the coldest and densest water mass in the world ocean. More than 60% of it is formed in the Atlantic sector of the Southern Ocean, i.e. in the Weddell Sea (Orsi et al., 1999), making it a key region for the deep and cold branch of the global thermohaline circulation. At the southern and western margins of the Weddell Basin, the precursors of AABW, Weddell Sea Deep and Bottom Water (WSDW and WSBW), are produced by interaction of warmer mid-depth and surface water masses with different shelf water types (see below, Fig. 3). The latter are partly generated by interaction with the Antarctic ice shelves and are, apparently, extremely sensitive to climate variability, which affects sea ice conditions and might alter basal melt rates or even induce ice shelf decay.

High Salinity Shelf Water (HSSW, salinities typically above 34.7 and potential temperature θ near the surface freezing point $T_f \approx -1.9°C$) is formed by brine rejection during sea ice production on the broad shelf regions of the south-western Weddell Sea during winter. It can become dense enough to reach the bottom, as reported from the western Weddell Sea (Gordon, 1998). Moreover, HSSW can mix with Warm Deep Water (WDW, with $\theta > 0°C$, advected into the Weddell Basin from the Antarctic Circumpolar Current) and Winter Water (WW, a remnant of the winter mixed layer), to produce Weddell Sea Bottom Water (WSBW, $\theta < -0.7°C$). This process is often referenced to as the Foster-Carmack process (e.g. Foster & Carmack, 1976).

Concurrently, HSSW, which flows into the caverns below the ice shelves, melts the ice from below (enhanced hydrostatic pressure at the base lowers the freezing temperature) or at its

front. The blend of glacial melt water and HSSW, called Ice Shelf Water (ISW, with θ below surface freezing temperature), mixes further with WDW or mWDW (i.e. WDW modified by WW) to produce WSBW as well. That process is usually referred to as the Foldvik process (e.g. Foldvik et al., 1985). Further mixing with ambient water masses (Foster & Carmack, 1976) or additions from external sources (Hoppema et al., 2001) renew Weddell Sea Deep Water (WSDW, -0.7°C < θ < 0°C).

WSBW is known to be formed in the southern Weddell Sea, partly in interaction with the Filchner-Ronne Ice Shelf (FRIS). Based on observations in front of the FRIS, Foldvik et al. (2004) described plumes of ISW flowing out from the Filchner Depression on distinct pathways northwards down the slope into the deep Weddell Basin, or following the continental slope westward. Using current meter data they estimate an outflow of cold water (θ < -1.9°C) of 1.6 ± 0.5 Sv (1 Sv = 10^6 m^3/s). Due to further entrainment of adjacent water they deduce a WSBW formation rate of 4.3 ± 1.4 Sv (θ < -0.8°C). However, the characteristic cold temperature of the ISW outflow is eroded rapidly when it leaves the Filchner Depression, as can be seen on sections across the slope west of the Filchner Depression. Further to the west, on the broad shelf in front of the Ronne Ice Shelf, HSSW is the dominating water mass. Weiss et al. (1979) and Nicholls et al. (2003) observed ISW also at the Ronne Ice Front, but from this source ISW could not be traced further northward into the Weddell Basin.

Still under consideration is the capability of the western ice shelf areas along the Antarctic Peninsula, particularly the Larsen Ice Shelf (LIS), to contribute to WSBW formation. Fahrbach et al. (1995) report WSBW formation by mixing of deep water with a flow originating from the shelf in front of the LIS. Weppernig et al. (1996) found evidence that this water contains significant fractions of ISW, possibly of LIS origin. Mensch et al. (1998) calculated a total WSDW and WSBW formation (θ < 0°C) of 5 Sv originating from the western Weddell Sea. Nicholls et al. (2004b) report ISW formation in the western Weddell Sea by basal ice shelf melting induced by modified WDW, pre-conditioned during winter, but not by HSSW. The issue of glacial melt water contributions to WSBW formation in the western Weddell Sea is of special interest, considering the decay of Larsen A and B in 1998 and 2002, respectively, (caused by increased basal melt rates, Shepherd et al., 2003) and in view of climate variability and increasing deep and bottom water temperatures as reported by Robertson et al. (2002), Schröder et al. (2002), and Fahrbach et al. (2004).

Useful tools to identify glacial melt water (or ISW) are the low-solubility noble gases helium (He) and neon (Ne) (Schlosser, 1986). Atmospheric air with a constant composition of these noble gases is trapped in the ice matrix during formation of the meteoric ice. Due to the enhanced hydrostatic pressure at the base, these gases are completely dissolved in the water, when the shelf ice is melting from below. This leads to an excess of $\Delta^4He = 1060\%$ and $\Delta Ne = 770\%$ in pure glacial melt water (Δ stands for excess over an air-water solubility equilibrium) (Hohmann et al., 2002). With an accuracy of 0.5% for ^4He measurements, melt water fractions of 0.05% are detectable by this method.

In ISW observed within the Filchner Depression the helium excess was about 20% (Schlosser et al., 1990), equivalent to a fraction of roughly 1.4% pure glacial melt water (assuming a background Δ^4He in the adjacent water masses of about 5%). In front of the Filchner Depression the ^4He excess was still as high as 10% (glacial melt water $\approx$ 0.5%). From Ice Station Weddell in 1992 (subsequently referred to as ISW-1), drifting east of the Antarctic Peninsula, Weppernig et al. (1996) used ^4He and oxygen isotope observations to estimate the fraction of ISW in WSBW ($\theta < -0.7°C$). They found 15% ISW, originating from the Filchner Ronne Ice Shelf, at the southern end (72°S) of the drift track, generally decreasing as the drift track progresses northward. But two anomalies of elevated ISW (glacial melt water) fractions were detected along the track. These were observed in the vicinity of Larsen C Ice Shelf (68.5°S) and at the northern end of the Larsen Ice Shelf. Based on the previously reported ISW outflow of 1 Sv from the Filchner Depression (Foldvik et al., 1985) Weppernig et al. (1996) estimated a WSBW formation rate of 5 Sv, including 10% ISW of Filchner Ice Shelf origin.

Particularly at mid-ocean ridges of the deep Pacific, additional ^3He (and less ^4He) is released into the deep water, resulting in an enhanced $^3He/^4He$ ratio of about 8 times the atmospheric ratio (Well et al., 2001). These waters contribute to Circumpolar Deep Water (Well et al., 2003), and hence to WDW, which then has a maximum $^3He/^4He$ ratio and slightly enhanced ^4He values. Neon provides complementary information (Rodehacke et al, 2006). In contrast to helium, neon has no internal sources (Well & Roether, 2003) other than glacial melt water, and has minimum values in WDW (see below, compare Figs. 5B and 5C, and the grey arrow in Fig. 2 pointing to the ^4He shift off the atmospheric $^4He/Ne$ ratio particularly in the WDW range that originates from Circumpolar Deep Water).

The chlorofluorocarbons CFC-11 and CFC-12 are age tracers due to their temporal evolution in the atmosphere and in the ocean surface waters. They allow estimating transit times of recently ventilated waters in the ocean interior, depicting the transport of these water masses (Weiss et al., 1985; Bullister, 1989).

There is only limited knowledge about the western Weddell Sea and, particularly, the Larsen Ice Shelf concerning WSBW formation processes and rates. One aim of the ISPOL experiment (RV Polarstern cruise ANT XXII/2, October 2004 to January 2005) was to find evidence for glacial melt water originating from LIS. A comprehensive description of the ISPOL cruise, the drift track and the ice conditions, is given by Dieckmann et al. (2007); see also Hellmer et al. (2006) and Hellmer et al. (2008). Absy et al. (2008) focus on the hydrography of the upper water column and a comparison with ISW-1. Here we analyze the formation of WSBW and quantify glacial melt water fractions by using hydrographic and tracer observations. We find clear evidence of an ISW/glacial melt water source at the Antarctic Peninsula – most definitely related to the LIS. This water can be traced further downstream along the slope towards the northern tip of the Antarctic Peninsula between 1000 m and the base of the slope.

In the following sections we describe the sampling and measurement of the presented data and the applied methods. Subsequently we analyze these observations and show how they relate to previous observations up- and downstream of the ISPOL investigation area. Thereafter, we deduce the fractions of the contributing water masses and the formation and export rates of WSBW.

2. Data and Methods

The location of the ISPOL experiment is shown in Figs. 1A and 1B. Heavy sea ice conditions during November prevented RV Polarstern to proceed further southwest and close to the continental shelf. A canyon located further south (69.5°S), suspected to be a possible pathway of locally formed ISW, was missed. Another canyon further towards the northwest (67°S) was not found, presumably due to unreliable charts; CTD observations differed partly by more than 200 m from the charts (Dieckmann et al., 2007). The southern end of the ISPOL drift coincided with an area where Weppernig et al. (1996) found enhanced ISW fractions near Larsen C (68.5°S, 100 km east of the ISPOL drift track). Furthermore, the cruise was designed as a drift

station, with RV Polarstern permanently attached to an ice floe. Due to a slow drift with several loops, the station drifted northwards only by a distance of 150 km during 38 days. Hence, the Larsen C Ice Shelf front was not covered completely.

[Figure 1A, 1B]

An additional CTD system carried by helicopter complemented the ship-operated profiling especially west of the drift track. It was equipped with a single Niskin bottle to get a water sample from each helicopter station close to the bottom. The obtained accuracies were 0.002 (salinity), 0.002°C (temperature), and 2dbar (pressure) for the ship based CTD and 0.005 (salinity), 0.003°C (temperature), and 3dbar (pressure) for the helicopter CTD (Absy et al., 2008).

In total, 300 samples from 29 ship casts and 20 bottom samples from helicopter stations were analyzed for helium isotopes and neon. All samples were stored in gas-tight copper tubes and analyzed mass spectrometrically at the IUP Bremen (Sültenfuß et al., 2007). The accuracy of measurements is 0.01 nmol/kg or 0.5% for ^{4}He, 0.04 nmol/kg or 0.5% for Ne, and 0.2% for the ^{3}He/^{4}He ratio. Replicate samples gave an error of the reproducibility of 0.5% for ^{4}He, 0.2% for Ne, and 0.1% for ^{3}He/^{4}He. However, the observed scatter of the ^{4}He and Ne measurement is larger (2% for ^{4}He and 1% for Ne within restricted density intervals). We assume that this apparent scatter reflects true variations within the water masses.

Because uncertainties in the solubility functions of helium and neon still exist (Weiss, 1971; see also Rodehacke et al., 2006) and because of non-linear effects, we use concentrations (nmol/kg = 2.2414 x cm^{2}STP/g) rather than the excess above the equilibrium concentration (e.g. Δ^4He = 100 x ($^4He_{obs}/^4He_{eq}$ – 1) in % where $^4He_{eq}$ = f(θ,S) is the solubility function of Weiss, 1971). The helium isotope ratio (^{3}He/^{4}He) is expressed in the common delta notation (δ^3He = 100 x ($[^3He/^4He]_{obs}/[^3He/^4He]_{atm.}$– 1) [%]). ^{3}He components from tritium decay are presumably negligible (Roether et al., 1998, Roether et al., 2001).

A total of 470 water samples from 29 ship casts were analyzed for CFC-11 and CFC-12. The samples were collected into 100 ml glass ampoules after flushing them with seawater for several minutes, and were flame-sealed under a flow of CFC-free nitrogen. The amount of CFC degassing into the headspace was accounted for during the measurement procedure. The CFC

measurement, at IUP Bremen, used a purge and trap sample pre-treatment followed by gas chromatographic (GC) separation using a capillary column and electron capture detection (ECD) (Bulsiewicz et at., 1998). The accuracy of the measurement is better than 1.5% or 0.04 pmol/kg for CFC-11 and 1.5% or 0.03 pmol/kg for CFC-12 (which ever is greater). CFC concentrations are calibrated on SIO98 scale (Prinn et al., 2000).

For comparison with the atmospheric source, the CFC concentrations are converted to partial pressure (ppt, parts per trillion) using the solubility function of Warner and Weiss (1985). For the southern hemisphere atmosphere we used the values of Walker et al. (2000), extended beyond the year 2000 using values from http://gaslab/ucsd.edu/pub/cfchist and followed up by a linear extrapolation into 2004.

We also use noble gas and chlorofluorocarbon measurements from previous cruises (Fig. 1A) for comparison with the ISPOL data. Helium isotope, neon, and CFC measurements are available on sections in the southern Weddell Sea (ANT XII/3, 1995, measured by the IUP Bremen tracer group as described above); (a) following the Filchner-Ronne Ice Shelf edge, (b) crossing the northern Filchner Depression, and (c) traversing the continental slope. While noble gas measurements are of comparable quality to those from ISPOL, the CFC measurements are less precise (CFC-11 ± 7% and CFC-12 ± 3%, due to the first application of flame-sealed CFC sample method). Since the ISW core in the Filchner Depression is not captured by our noble gas measurements, we use earlier measurements of Schlosser et al. (1990). The Weddell Sea transects from Joinville Island into the Weddell Basin (ANT XIII/3 in 1996 and ANT XV/4 in 1998; hereinafter termed JV section), also provide both noble gas and CFC measurements. All these measurements were obtained by the IUP Bremen tracer group; since in these cases the CFC samples were measured on board, the accuracy is better than 1% or 0.02 pmol/kg for CFC-11 and 1% or 0.01 pmol/kg for CFC-12. All noble gas measurements performed at the IUP Bremen were corrected for small systematic errors due to the variability of the calibration standard. These adjustments were obtained by the analysis of crossing points of the sections. The corrections are listed in Table 1.

[Table 1]

The ISPOL ^{4}He and Ne values are systematically higher compared to the data of previous sections from the southern and northwestern Weddell Sea (ANT XII/3, ANT XIII/4, and ANT

XV/4). This inconsistency is believed to be caused by a calibration problem in the measurement. Therefore, and because the ISPOL data set is fully consistent internally, we applied an adjustment of -0.6% for ^{4}He and -1.9% for Ne (based on a comparison between ISPOL data and previous sections for samples with $32.50 < \sigma_1 < 32.55$, see Figs. 5; σ_1 = potential density [kg/m^3] referenced to 1000 dbar). With this adjustment, the ^{4}He/Ne ratios fit to all other observations from the Weddell Sea perfectly (Fig. 2). The helium offset from the atmospheric ratio (grey line in Fig. 2), most apparent for all data sets in the WDW range (indicated by the grey arrow at $\Delta Ne \approx 3\%$), originates from small helium additions from Pacific deep waters. Note, however, that these adjustments reduce the ^{4}He and Ne values, and thus, also the deduced fractions of glacial melt water. The uncorrected data would lead to implausibly high glacial melt water fractions.

[Figure 2]

We apply an Optimum Multiparameter Analysis (OMP; Tomczak, 1981; Tomczac and Large, 1989; Hinrichsen and Tomczak, 1993) to deduce the contributing fractions of the four source water masses (WW, WDW, HSSW, and glacial melt water) to deep and bottom water formation. Fig. 3 represents the mixing scheme according to the "Foldvik process" (dashed line) and the "Foster-Carmack process" (dotted lines) in θ/S and θ/^{4}He parameter space, and illustrates how helium observations provide complementary information.

[Figure 3]

The OMP is based on an over-determined system of constraining linear equations. The first equations represent the mixture of source water masses by linear combinations of the fractions f_i of the source water masses and their characteristic properties X_i (like θ, S, and tracers). The last equation ensures mass conservation. In the optimum case this results to the observed properties X_{obs} of the analyzed water mass (Eq. 1).

$$X_{obs} = \Sigma\, f_i\, X_i \qquad (1)$$

Inverting this equation system (minimizing the deviations between observed and computed properties in a least square sense) yields the optimum combination of source water fractions. The system of equations is normalized by the mean and the range each property spans to

account for their different orders of magnitude and, furthermore, it is weighted by the average uncertainty of each property to account for the different signal-to-noise ratios.

We use the residuals R between observed and computed properties of the analyzed water mass as a qualitative measure of the OMP. Furthermore, we test the OMP result 1) by individual variation of each source water mass property within its respective uncertainties and 2) by statistical variation of the properties of the analyzed water mass within their errors. The resulting deviations are summed up by error propagation and are considered as the uncertainty of the fractions.

Chlorofluorocarbons (CFCs) are transient tracers due to their atmospheric time evolution (Walker et al., 2000). Atmospheric concentrations of the entirely anthropogenic CFC-11 and CFC-12 increased almost steadily between the 1940s and the 1990s. More recently they leveled off (CFC-12) or decreased (CFC-11). They enter the ocean by gas exchange across the atmosphere-ocean interface. If the surface water were in equilibrium with the atmosphere and no mixing and internal sources or sinks altered the CFC partial pressure in the ocean interior, the "age" (i.e. the time elapsed since the water parcel has left the surface layer) would be the time difference between the observed CFC partial pressure and the corresponding value in the atmospheric time history (Weiss et al., 1985; Bullister, 1989). This first-order concept of determining a transit time is termed "concentration age".

Since surface water is generally not in equilibrium with the atmosphere (due to reduced gas exchange by ice cover or faster downward mixing than gas transfer), the saturation, i.e. the ratio between the observed and the equilibrium concentration, has to be considered. It is also required to account for the apparent saturation in subsurface water masses, if they are used as source water masses (Karstensen and Tomczak, 1998). Furthermore, if the water mass was separated from the surface for a certain time Δt before it got re-involved in the inner oceanic circulation, one can account for that delay by considering an enhanced apparent saturation (Eq. 2):

$$S = CFC_{obs} / CFC_{atmos}(t_{obs} - \Delta t) \qquad (2)$$

Due to a slightly different solubility for the two CFCs and their non-uniform and non-linear temporal evolution in the atmosphere, these apparent saturations are generally not identical and

vary in time (Beining and Roether, 1996). However, significant deviations from the true age are more likely related to mixing (partly with tracer free water), which generally leads to an underestimate of the real age (Sonnerup, 2001; Waugh et al., 2003).

3. Observations

Fig. 4 shows vertical sections of ^{4}He, δ^3He, and CFC-12 along the main ISPOL drift track (about parallel to the meridional θ and S sections shown in Absy et al., 2008). The ^{4}He section appears to be more scattered than those of δ^3He and CFC-12, which is due to the lower dynamic range of ^{4}He. However, the ^{4}He section shows increasing values towards the bottom with a maximum in the WSBW layer ($\theta < -0.7$°C) several 10 meters above the bottom, indicating large glacial melt water contributions. The δ^3He values have a maximum in the WDW layer ($\theta > 0$°C and 500 to 1000 m depth in the south with an uprising lower boundary as stations get shallower towards the north). Towards the bottom they approach surface layer values. CFC-12 partial pressure shows maximum values at the surface, due to its atmospheric source, and increasing values towards the bottom, due to increasing fractions of recently ventilated (surface) water. Extreme values of θ, ^{4}He, δ^3He, and CFC-12 close to the bottom are apparent along the whole section even in the shallower northern part, indicating a similar composition of source water masses along the entire drift track.

[Figure 4]

Property plots versus θ for the ISPOL cruise are displayed in Figs. 5. Observations in front of the Filchner Depression (sub-section b and c), and downstream (JV sections west of 45°W) are included for comparison (for locations of sections see Fig. 1A). The ISPOL WW layer is characterized by the surface freezing point temperature (Fig. 5A). WDW temperatures and salinities from the ISPOL site are slightly colder and fresher than those along the JV sections, while observations from the southern Weddell Sea show warmer and fresher WDW values, each reflecting the different distances from the WDW core and its source.

[Figure 5A, 5B, 5C, 5D, 5E]

At the bottom, ISPOL temperatures decrease to a minimum of -1.9°C and salinities reach values of 34.63. An evident feature is the sickle-shaped intermediate salinity minimum in the upper layer of WSBW (-1.5°C < θ < -0.7°C, S ≈ 34.60, indicated by the thick arrow in Fig. 5A). This salinity minimum can be explained by admixtures of glacial melt water or entrainment of WW (or mWDW). The reduction in salinity of about 0.04 (the difference between the intermediate minimum and a straight line between WDW and coldest WSBW) would require an admixture of roughly 0.1% pure glacial melt water (S = 0). The colder, deeper WSBW layer (θ < -1.5°C) contains larger admixtures of HSSW. The ISPOL bottom water temperatures are considerably lower than those observed during ISW-1, even where helicopter CTD stations overlap the ISPOL drift track (ISW-1 temperature minimum around -1.4°C, data not included in Fig. 5A). The temporal changes in bottom water θ/S characteristics are discussed in detail by Absy et al. (2008).

WSBW along the JV section is systematically warmer and slightly saltier, causing a lifting of the sickle-shape in the θ/S space (thin arrows, Fig. 5A). On the slope, WSBW has a minimum temperature of -1.4°C, which indicates further exchange with WSDW. Off the slope, in the inner basin, the bottom water is even warmer (minimum at -0.9°C), and the intermediate salinity minimum appears to be eroded. The sickle-shaped WSBW θ/S characteristic was previously observed by Fahrbach et al. (1995) west of the Larsen Ice Shelf and in the western part of the JV section. They argued that the low salinity WSBW originates from the western Weddell Sea while the higher bottom salinities originate from the south.

In the bottom layer of the Filchner Depression temperatures are below the surface freezing point T_f due to admixtures of outflowing ISW plumes. Highest salinities (S > 34.65, with θ ≤ T_f) represent remnants of HSSW, originating from the southwestern shelf. Temperature and salinity data directly within the Filchner outflow (subsection b, diamonds in Fig. 5A) are comparable with the bottom water properties observed at the ISPOL site. However, water flowing out the Filchner Depression along the southern slope towards the west (across subsection c, open circles in Fig. 5A) rapidly changes characteristics (θ > -1.65°C). Hence, the Filchner outflow and the bottom water characteristics at the ISPOL site cannot be connected. Therefore, an additional bottom water source exists in the western Weddell Sea that, at least intermittently, supplies cold and dense water of different characteristics which cause the sickle-shape in θ/S space.

Both ^{4}He and Ne in the surface layer and in the WW layer from the ISPOL site are elevated in comparison to air-sea equilibrium values (Figs. 5B and 5C, Δ^4He = +3.5%, and ΔNe = +2%). Such an excess can be explained by glacial melt water additions from frontal melting of shelf ice or icebergs, while the stratification and the sea ice cover prevents equilibration with the atmosphere. It cannot completely be caused by upwelling WDW, since Ne has a minimum in WDW (Fig. 5C). Appart from considerable data scatter, the ^{4}He and Ne maxima in the upper WSBW layer ($\theta \approx$ -1.4°C) evidently coincide with the intermediate salinity minimum (thick arrow in Fig. 5A). The large excesses of Δ^4He and ΔNe (+10% and +8% relative to air-water equilibrium) are only achievable by the addition of glacial melt water. The coldest bottom layer shows more moderate ^{4}He and Ne values, indicating enhanced HSSW components which carry smaller concentrations of ^{4}He and Ne. Such a decline of helium and neon towards the bottom was previously reported by Weppernig et al. (1996) from the southern-most ISW-1 stations, which show a tongue of HSSW extending from the continental shelf to the lower continental slope.

The ISPOL ^{4}He and Ne maxima in WSBW (Figs. 5B and 5C) are quite similar (Ne slightly higher) to those in out-flowing water within the Filchner Depression (subsection b in Fig. 1A, diamonds in Figs. 5B and 5C). However, in the ISPOL data the noble gas maximum is about 0.5°C warmer than in the Filchner outflow (coinciding with the salinity minimum at around -1.4°C). Furthermore, west of the Filchner Depression (subsection c in Fig 1A, open circles in Figs. 5B and 5C), such high ^{4}He and Ne values are no more present. This means that both temperature and noble gas characteristics are dispersed rapidly after the Filchner outflow turns west along the slope. These observations provide support that the western Weddell Sea has its own source (possibly intermittent). Along the JV section, the helium and neon values lie almost on a straight line between WDW, WSDW, and the lower WSBW values observed at the ISPOL site. That means that the extreme helium and neon values observed in upper ISPOL WSBW are an effect of a strong (possibly intermittent) melt water plume and are eroded on the way northward by further mixing with WSDW.

The ISPOL δ^3He data (Fig. 4B, and Fig. 5D) exceed the low values from the area around the Filchner Depression (δ^3He < -2%, $\theta < T_f$). West of the Filchner Depression ($\theta > T_f$) the bottom water values are in the order of 1%, while the ISPOL bottom water values are between 1% and 2%. WW values at the ISPOL site are near to 0% and are, thus, larger than equilibrium values (-1.8% at $\theta = T_f$); δ^3He rich WDW (up to 8%) is admixed into the surface layer, while the ice

cover prevents equilibration with the atmosphere. From these observations we deduce a WDW entrainment of 18% into the surface mixed layer. This value agrees very well with the findings of Weppernig et al. (1996), located 100 km east of the ISPOL site. In the vertical δ^3He distribution (Fig. 4B) it can be seen that remnants of WDW reach relatively shallow areas in the northern part of the drift track.

CFC-12 data are displayed in Fig. 4C and Fig. 5E. Surface mixed layer values reveal a well-mixed water body with a saturation of 70% (68% for CFC-11). These are typical surface layer values for the western Weddell Sea (e.g. Huhn et al., 2001). The CFC minimum on the WDW ($\theta \approx 0.4$°C) from our observations in the western and northwestern Weddell Sea (i.e. ISPOL and JV sections) increases continuously from roughly 15 ppt (1996) to 25 ppt (1998) and 35 ppt (2004), reflecting the atmospheric CFC evolution and the renewal of WDW due to the upwelling of CFC-richer and younger WSDW. CFC values in the bottom layers are only slightly lower than in the near-surface layers (WW) for all data sets, indicating recent ventilation of the bottom layer.

A special feature is the low CFC-12 values (≤ 50 ppt) for part of the WSDW temperature range at the Filchner and JV sections. These values are found rather more off-slope, representing the transition into the off-slope CFC minimum in that range described by Hoppema et al. (2001). These authors found the decrease to become prominent where the bottom depth begins to exceed roughly 1500 m, which explains the virtual absence of the feature in the ISPOL region.

At the ISPOL site the CFC values in WSDW ($-0.7 < \theta < 0$°C) lie on an almost straight mixing line between the minimum in WDW and the maximum in the lower part of WSBW. In the upper ISPOL WSBW (indicated by the arrow in Fig. 5E), however, the CFC values are slightly higher than according to the mixing line. This enhancement coincides with the salinity minimum (sickle, Fig. 5a) and the noble gas maxima (Fig. 5B and 5C) noted above. It consistently reveals the entrainment of near surface water masses (WW or mWDW) into this layer, and demonstrates that this layer is not only a mixture of deep WSBW and WSDW. These findings also point to a source rather near-by.

The horizontal distributions of properties in the bottom layer at the ISPOL site are shown in Fig. 6. Anticipating a continuous flow with contributions of glacial melt water (discharged from the western shelf or from the canyon further south indicated by bathymetry maps), one would

expect a consistent pattern of highest ^{4}He and Ne concentrations and of lowest temperatures (and highest densities) in the south or west with a gradient towards the north and down the slope. But the property distributions in the bottom layer are patchy and not fully consistent, so that only weak patterns can be recognized. This patchiness may be partly caused by the projection of the irregular distributed observations on a regular grid, causing artificial structures where observations are extremely sparse or dense (but not synoptic). Furthermore, for ^{4}He and Ne the signal-to-noise ratio is low due to the small range of values.

[Figure 6]

However, the patchiness also indicates that the area is probably subject to a complex flow pattern in space and time. Two parallel, seemingly unconnected branches of lower temperatures seem to evolve from southwest ($\theta \approx -1.8$°C) down the slope to the northeast (dashed and dash-dotted arrows in Fig. 6). The salinity distribution shows a gradient of high ($S > 34.64$) to low salinities ($S \approx 34.61$) in northeast direction with two areas of lower salinities around 55.5°W in the south and 56.3°W in the north. These low-salinity patches roughly coincide with an almost unbroken band of low noble-gas values (dashed line), but are not reflected by any similar structure in the temperature distribution. A consistent feature in all property distributions is a band, identifiable by relatively low temperatures and high noble gas values, leading from about 56°W/68°S downslope towards the northeast (dashed arrow) highlighting a likely path of glacial melt water enriched bottom water.

4. Discussion

4.1. Shelf water contributions to deep and bottom Water observed in western Weddell Sea

For WSDW and WSBW formation we account for four parent source water masses: WW, WDW, HSSW, and glacial melt water (see Fig. 3). We do not account for mWDW, a mixture of WW and WDW, nor ISW, a mixture of HSSW and glacial melt water. We employ an Optimum Multiparameter Analysis (OMP) using θ, S, ^{4}He, Ne, and the ^{3}He/^{4}He ratio (i.e. δ^3He) to calculate the relative fraction of each of the four source water masses in the deep and bottom water observed at the ISPOL site. We define the source water masses within limits of temperature, salinity, and density and calculate means and standard deviations of their

properties from the available observations. As limits we use standard values from the literature (e.g., Carmack and Foster, 1975); if necessary, we carefully adjusted and complemented these limits for better characterisation and distinction of the source water masses on basis of the available observations (Fig. 5A, see also Fig. 7). The used definition limits, the characteristic (mean) values, and their uncertainties are summarized in Table 2. CFC measurements are used later to infer the transit times of the source water mixture.

[Table 2]

As "uncertainties" of the characteristic values in Table 2 we use the standard deviation of the individual measurements rather than the error of the mean (the accuracy of the measurement is mostly smaller). These generally larger "uncertainties" are used to account for the range the parameters usually cover within the water masses (e.g., θ within WDW). Furthermore, these larger uncertainties better characterize the true variability within the water masses. Since ^{4}He and Ne values for glacial melt water are based on measurements of the air content in meteoric ice from different locations (Hohmann et al. 2002) we used as their uncertainties the standard deviation of these air measurements. For weighting the OMP to account for the different signal-to-noise-ratios of the used properties one has to apply uniform errors for each property. We use average uncertainties of $\varepsilon_\theta = 0.1°C$, $\varepsilon_S = 0.03$, $\varepsilon_{4He} = 1\%$, $\varepsilon_{Ne} = 1\%$, $\varepsilon_{\delta 3He} = 0.4\%$ (Table 2). The property distributions of the ISPOL data and the characteristic values of the source water masses (within their uncertainties) are compared in Fig. 7.

[Figure 7]

The results of the OMP (separately obtained for each ISPOL data point within WSDW and WSBW, pink dots in Fig. 7) are displayed in Fig. 8. The OMP-derived fractions of glacial melt water in WSDW and WSBW range from around 0% to a maximum of 0.4%. These values are small but significant. They are compatible with the rough estimate based on the intermediate salinity minimum (see above) and well comparable to values in front of the Filchner Depression reported by Schlosser et al. (1990) derived from ^{4}He observations alone (melt water fractions up to 0.5%). The values are significant, in that the estimated OMP error for the melt water fractions is only around 0.03% (see below), similar to the uncertainty in the Schlosser et al. (1990) study (0.05%). That means that the glacial melt water is well traceable by the applied

method. Moreover, assuming a total dense-water formation rate of 1 Sv, a melt water fraction of 0.1% corresponds to the rather considerable melt rate of more than 30 Gt/year.

[Figure 8]

A general trend of increasing melt water fractions with decreasing temperature is evident (from 0.07% in the upper WSDW to 0.12% in the lower WSBW according to a linear regression versus θ, the solid blue line in Fig. 8). Apparently, the deviations of individual fractions from the regression line (standard deviation of individual fractions from regression line ≈ 0.06%) are due to variability within the composition of the observed WSBW rather than to the uncertainty of the determination (uncertainty of individual fractions ≈ 0.03%, see below). However, in the mid-range WSBW around -1.4°C, where ^{4}He and Ne are highest and the salinity has its intermediate minimum, several individual melt water fractions exceed the trend considerably. As expected, the glacial melt water fractions are strongly correlated with the constraining parameters ^{4}He and Ne (Table 3). Correlations with the other parameters are weak.

[Table 3]

Fractions of WDW decrease with decreasing temperature from almost 90% at the boundary between WDW and WSDW (0°C) to close to zero for the lowest temperature (r = 0.95). The regression of WDW vs. θ represents the individual fractions quite well (mean deviation from the regression < 1%). The WDW fractions do not reach 100% at the WDW/WSDW boundary, since the WDW properties are not defined directly at the boundary but in the core of WDW at θ ≈ 0.35°C. Additionally to the strong θ correlation with θ (Table 3), there is an extremely strong correlation with δ^3He.

The HSSW and WW fractions also increase, similar to the glacial melt water fractions, with decreasing temperature. The correlation of the HSSW fractions is negative with θ, positive with ^{4}He and Ne, and weakly negative with S. This is surprising, since salinity is the most characteristic property of HSSW so that one would expect an increase of the HSSW fraction with increasing salinity. However, the computed correlation in Table 3 holds for the whole WSDW/WSBW layer. In the lowest part of the WSBW range, i.e. below the intermediate salinity minimum (see Fig. 5A), the correlation between the HSSW fractions and salinity is positive. This demonstrates the sensitivity of the OMP to the complexity of the water mass

composition and, furthermore, the necessity of using different properties that provide independent information.

The WW fractions are strongly correlated with θ, S, and δ^3He. For temperatures around -1.4°C the WW fractions show a slight maximum. This supports consistently our previous result that the upper WSBW layer (coinciding with the local salinity minimum and ^{4}He and Ne maxima) received larger admixtures of melt water and WW. When the melt water leaves the sub-ice cavity, it is stratified in a relatively thin layer at mid-depth, deep enough to be separated from the surface mixed layer to prevent the gas exchange with the atmosphere (so that additions of helium and neon from molten ice are conserved) but shallow enough to entrain WW or mWDW.

A measure of the OMP quality is the residuals between the observed and deduced properties: The values obtained, R_θ = 0.07°C, R_S = 0.001, R_{4He} = 0.007 nmol/kg, R_{Ne} = 0.025, $R_{\delta 3He}$ = 0.33%, and $R_{conservation\ of\ mass} \approx 0$, are comparable or even smaller than the parameter uncertainties (Table 2). As a further test of the sensitivity of the OMP we varied separately all source water parameters within their uncertainties (Table 2) and the observed WSDW and WSBW properties within their errors. By combining the resulting deviations from the unvaried case by error propagation we get a measure of the uncertainty of the computed source water fractions (in absolute %): glacial melt water ± 0.03, WW ± 5, WDW ± 3, HSSW ± 5. Varying only ^{4}He and Ne values of glacial melt water within their uncertainties, the glacial melt water fractions vary in the order of 0.01 (absolute %). These uncertainties are smaller than the scatter of the individual fractions around the temperature regression lines. Using excess Δ^4He and ΔNe instead of the concentrations ^{4}He and Ne in the OMP we get glacial melt water fractions which are about 0.01 to 0.02 (absolute %) larger, due to the non-linearity of the solubility of the gases. This "overestimate" is on the order of 20% (relative), similar to the 25% estimated by Hohmann et al. (2002) for this effect.

We applied the same OMP approach for ISW as a source water mass instead of glacial melt water and the same HSSW properties as used by Weppernig et al., 1996 (in lack of direct ISW observations in the western Weddell Sea we use the ISW properties observed in the Filchner Depression adopted from Schlosser et al., 1990, see Table 2). The OMP derived mean ISW fraction in WSBW is 12%, ranging between 0% and about 45%. Not surprisingly, the HSSW fractions are accordingly lower because ISW is a mixing product of HSSW and glacial melt

water. These findings are fully compatible with the value found by Weppernig et al. (1996) for the Ice Station Weddell (ISW-1) section at about 68.5°S and demonstrate the validity of our approach.

The CFC observations agree very well with the above findings. To demonstrate this, we apply an approach similar to Karstensen and Tomczak (1998). We reconstruct the CFC partial pressure history in WSBW (Eq. 3), accounting for the contributing fractions of each source water mass f_i (from the regression lines in Fig. 8 for a given temperature) and their apparent CFC saturation S_i (Table 2). As a first approach we assume constant apparent saturations. The time dependence of the reconstructed CFC history in WSBW is then given by the time dependence of the atmospheric histories.

$$CFC_{WSBW}(\theta,t) = CFC_{surf}(t) \cdot$$
$$[S_{WW} \cdot f_{WW}(\theta) + S_{WDW} \cdot f_{WDW}(\theta) + S_{HSSW} \cdot f_{HSSW}(\theta) + S_{ISW} \cdot f_{\text{glacial melt water}}(\theta)] \quad (3)$$

The CFC observations (separately for potential temperature intervals -1.9°C < θ < -1.4°C and -1.4°C < θ < -0.7°C in Fig. 9) are fully compatible with the reconstructed CFC histories (calculated for θ = -0.7°C, -1.4°C, and -1.9°C). The error of the reconstructed CFC histories (accounting for ½ σ of fractions f_i and ½ σ of saturations S_i) is in the order of 10%. A significant temporal shift from the reconstructed time histories (i.e., an age or transit time from the source to the area of observation) is not evident from these observations.

[Figure 9]

4.2. Export of WSBW across the JV section

On the JV section, WSBW (θ < -0.7°C) is confined to a relatively thin layer adjoining the slope (in the following referred to as on-slope WSBW) and to a 500 m thick layer in the inner basin (subsequently referred to as off-slope WSBW) (Fig. 10).

[Figure 10]

Rather high CFC values in the on-slope WSBW, to be observed between 1200 m and the base of the slope, indicate a recent ventilation. Fahrbach et al., (1995) assumed the origin of this on-

slope WSBW to be in the western Weddell Sea. As already discussed in Section 3, we conclude that the on-slope WSBW is associated with WSBW found in front of the Larsen Ice Shelf. In the off-slope WSBW CFC concentrations are considerably lower but still enhanced in comparison to the water further up (i.e. WSDW). The θ = -0.7°C boundary between WSDW and WSBW, coinciding with a strong gradient in the CFC profiles (Fig. 5E), lies below 4000 m depth, or 500 m above the bottom of the basin. ^{4}He and Ne values increase downwards in the water column and are highest in the deep and bottom water, but their scatter does not allow a distinction between on- and off-slope WSBW. δ^3He values in the on-slope WSBW are slightly lower than in the off-slope WSBW, which also indicates larger fractions of melt water or recently equilibrated surface water in the on-slope WSBW.

We employ the OMP approach to derive the source water fractions for WSDW and WSBW along the JV section, using the same source waters and their characteristic parameter values (Table 2) as previously applied for the ISPOL analysis. The result – separated for observations on and off the continental slope (separation at about 450 km off the shelf break) – is displayed in Fig. 11 (analogue to Fig. 8; for comparison the regression lines from the ISPOL site are included in Fig. 11 as thin lines).

[Figure 11]

The OMP-derived fractions of WW, WDW, and HSSW from the JV sections reach almost the same values and the same temperature regressions for both on-slope and off-slope stations (within their scatter). Even more, both sub-sets show almost the same trends as for the ISPOL site (thin lines), except that they are cut off at temperatures below -1.4°C (on-slope stations) and -0.9°C (off-slope stations) due to further mixing with water from above and further transformation of WSBW into WSDW on the way from the source to the JV section. The glacial melt water fractions (blue dotted and dashed lines) appear systematically smaller than at the ISPOL site (mean melt water fractions $\approx$ 0.04%). This shift might be an effect of the lower ^{4}He and Ne signal-to-noise ratio further off the sources (the derived melt water fractions are only slightly larger then their uncertainty) or of the temporal variability of the formation and the transport of the bottom water.

To estimate a transit time for newly formed WSBW from the western Weddell Sea to the on-slope JV section (and from the southern Weddell Sea to the off-slope JV section) we use the

CFC-based approach as for the ISPOL data above. We reconstruct the CFC history for WSBW (Eq. 3) with the computed source water mass fractions f_i for the JV section (separately for on-slope and off-slope WSBW from the regression lines in Fig. 11) and the related apparent CFC saturations S_i (Eq. 2). The latter are derived from observations at the ISPOL site for on-slope WSBW and from observations in the southern Weddell Sea, i.e., in front of Filchner Ice Shelf, for off-slope WSBW (Table 4). The reconstructed CFC-12 histories and observations from 1996 and 1998 along the JV section (west of 45°W only) are displayed in Fig. 12 for the respective θ ranges ($-0.7 \geq \theta \geq -1.4$°C for on-slope WSBW, and -0.7°C $\geq \theta \geq -0.9$°C for off-slope WSBW).

[Table 4]

[Figure 12]

The CFC age (i.e., the mean time lag between observed concentrations and the respective ones from the reconstructed history indicated by the arrows in Fig. 12) for the on-slope WSBW is 9 ± 3 years (the same age is obtained from CFC-11). The error accounts for the uncertainties of the saturations (Table 4) and the uncertainties of the fractions of the contributing source water masses, leading to an uncertainty in the reconstructed CFC histories of about 10%.

With a distance of 700 km (from 69°S following the slope towards the JV section), the transit velocity becomes 0.25 ± 0.1 cm/s, lower than from direct velocity observations. For instance, Fahrbach et al. (2001) observed a maximum velocity on the slope across the JV section on the order of 4 cm/s. The explanation is that, in contrast to the direct measurements, the tracer-derived age and velocity represent the long term mean transport of a water body, in this case the entire WSBW layer below the -0.7°C isotherm between the source (i.e. the western Weddell Sea ice shelf region) and the point of observation (JV section on slope) including mixing of flow trajectories (i.e. internal mixing and recirculation) and residence times (e.g. between the basal ice shelf melting with subsequent WSBW formation and its discharge).

With a mean thickness of the WSBW layer of 400 m (-0.7°C isoline down to the bottom, Fig. 10) and an extension of this layer 350 km off the shelf break, the cross-section is $140 \times 10^6 m^2$, yielding a total transport of on-slope WSBW of roughly 0.35 ± 0.15 Sv (the error accounts for the transit time error of 3 years) crossing the JV section below the -0.7°C isotherm. Upward

mixing of parts of the initially formed WSBW into the WSDW (the renewal of WSDW can be seen in the temporally increasing CFC content also in this water body) is not considered by this approach. The observed decrease of the steady-state tracer ^{4}He in WSBW along the slope (from 1.95 nmol/kg at the ISPOL site to 1.91 nmol/kg on the JV section) is an effect of this mixing (1.89 nmol/kg in the ambient WSDW). We use these values to estimate the fraction (γ) of the initially formed WSBW that reaches the JV section below the -0.7°C isoline (Eq. 4).

$$^4He_{JV\text{-}WSBW} = \gamma\ ^4He_{ISPOL\text{-}WSBW} + (1\text{-}\gamma)\ ^4He_{ambient\ WSDW} \qquad (4)$$

We find that γ = 1/3 of the initially formed WSBW arrives at the JV section (the same ratio is obtained from the Ne decrease). The remaining 2/3 are lost upwards and are replaced by WSDW. This corresponds to an initial WSBW formation rate in the western Weddell Sea of 1.1 ± 0.5 Sv. With this formation rate and the mean initial glacial melt water fraction of 0.1% (Fig. 8) we deduce the total melt rate at the base of the Larsen Ice Shelf to 35 ± 19 Gt/year. With an ice shelf area of roughly 100000 km^2 (mainly Larsen C), this corresponds to a melt rate of 0.35 ± 0.19 m/year. These uncertainties of the melt rates account for the uncertainties of the formation rate (± 0.5 Sv) and of the OMP derived melt water fractions (± 0.03%). However, one has to consider the intermittent nature of the flow, so that the melt water fraction (and γ) might be subject to even larger temporal variability, as indicated by the scatter of the single melt water fractions (the standard deviation of the individual melt water fractions from the regression line in Fig. 8 is about 0.06%, the total range is from 0.0% to 0.4%).

For the off-slope WSBW we get a mean CFC age of 22 ± 5 years (Fig. 12). With a distance between Filchner outflow and JV section of about 1200 km the mean transit velocity amounts to 0.17 ± 0.05 cm/s. Assuming a mean WSBW thickness of 500 m and a width of 1500 km (from 350 km off the shelf break in the northwestern Weddell Sea to 100 km off Kapp Norwegia, where the θ = -0.7°C isoline vanishes; see Fig. 10 and compare with Fahrbach et al., 2004) the cross-section is 750x10^6 m^2. This yields a transport of roughly 1.3 ± 0.4 Sv. If we assume the same 2/3 loss by upwelling 3.9 ± 1.2 Sv is formed in the southern Weddell Sea at the FRIS. For the 500000 km^2 of Filchner-Ronne Ice Shelf, this formation rate and a glacial melt water fraction of 0.1%, the melt rate amounts to 0.25 ± 0.11 m/year or 123 ± 53 Gt/year. The uncertainties account for uncertainties of the formation rate and the melt water fraction as described above. However, in this case the melt water fraction and γ might bear even larger

uncertainties and variability due to temporal fluctuations, so that the true range of the melt rate is probably larger.

Our derived WSBW formation and basal melt rates are in good agreement with previous findings. Foldvik et al. (2004) calculated from current meter data a total WSBW ($\theta < -0.8°C$) formation of 4.3 ± 1.4 Sv associated with the flow out of the Filchner Depression. The computed basal melt rates from Hellmer (2004) are 38Gt/year at the LIS and 120 Gt/year at FRIS. Even if our findings bear large uncertainties, they demonstrate the capability of our method, which is complementary to oceanographic or glacialogical estimates (Gammelsrød et al., 1994; Foldvik et al., 2001; Joughin and Padman, 2003) and independent of direct velocity measurements, which are difficult to carry out in this hardly accessible area. Thus, they provide – at least – an independent estimate of WSBW formation and basal melt rates.

The WSBW formed in the western Weddell Sea (it can be identified along the JV section on the slope up to 1200 m, see Fig. 4 and Fig. 10) is shallow enough that it might leave the Weddell Basin towards the north through the gaps in the South Scotia Ridge to supply AABW, keeping with trajectories of numerical floats that indicate the flow of dense water masses originating from the Larsen Ice Shelf through Philip Passage (Schodlok et al., 2002). The off-slope WSBW is generally too deep to follow that pathway.

5. Conclusions

One aim of the ISPOL experiment (RV Polarstern cruise ANT XXII/2, Oct. 2004 to Jan. 2005) was to find evidence for deep and bottom water formation in the hardly accessible area of the western Weddell Sea. Deep and bottom water formation processes and rates, particularly the role of the ice shelves at the Antarctic Peninsula and contributions of glacial melt water as well as basal melt rates, are rather unknown. Previous studies (Fahrbach et al., 1995, Weppernig et al., 1996; Mensch et al., 1998) suggested that the western Weddell Sea has to be considered as a distinct source for Weddell Sea Bottom Water (WSBW). The hydrographic and tracer observations obtained during ISPOL revealed recently ventilated bottom water which contains significant fractions of glacial melt water, most definitely originating from the Larsen Ice Shelf (LIS).

WSBW at the ISPOL site has low temperatures (θ < -1.8°C, Fig. 5A) and high noble gas concentrations (^{4}He > 1.96 nmol/kg or Δ^4He > 9% and Ne > 8.6 nmol/kg or ΔNe > 6% , Fig. 5B and 5C) even at the shallow northern stations (Fig. 4), which cannot be explained by the export of bottom water containing glacial melt water or Ice Shelf Water (ISW) from the Filchner-Ronne Ice Shelf (southern Weddell Sea), as the low temperatures and high helium values in the water spilling over the sill of the Filchner Depression are dispersed quickly on its way down and westwards along the slope. ISW observed in front of the Ronne Ice Front (southwestern Weddell Sea) does not penetrate further north (Nicholls et al., 2003), and HSSW observed in the southwestern Weddell Sea does not carry enough ^{4}He and Ne. Our observations provide clear evidence that the western Weddell Sea has its own, at least intermittent, source for bottom water formation. Figure 13 provides a schematic of the flow of the water masses formed at the two source regions and; it also includes our deduced WSBW formation and ice shelf basal melt rates.

[Figure 13]

One consistent feature of the ISPOL profiles is an intermediate salinity minimum coinciding with a layer of noble-gas enriched water occupying the upper part of WSBW (-1.4°C < θ < -0.7°C), while in the deepest layer (θ < -1.4°C) noble gas values are smaller and salinity is higher (Fig. 5A – 5C). This feature is also apparent in ISW-1 profiles close to the southern source and at the ISPOL site latitudes, but further to the east, as previously reported by Weppernig et al. (1996). It indicates an upper bottom water layer with higher admixtures of glacial melt water (or ISW), causing the observed high ^{4}He and Ne values, and of entrained WW (or mWDW), increasing the CFC content in this layer (Fig. 5E), contrasting with a bottom water layer, which contains higher fractions of HSSW, represented by the highest salinities but only slightly enhanced noble-gas and CFC values. This distinct stratification can be expected only close to the sources, since further mixing would leads to a more homogeneous distribution of steady-state properties in the deep and bottom waters as can be seen further of the ISPOL site on-slope and, particularly, off-slope along the Joinville section.

At the ISPOL site, observed bottom water temperatures were significantly lower and helium concentrations slightly higher than during ISW-1 (Gordon et al., 1993; Absy et al., 2008), located only 100 km further to the east but 1000 m deeper. The reason could be a temporally and spatially variable discharge of recently formed bottom water. Furthermore, one has to

consider that ISW-1 and ISPOL were performed as drift stations above rather unknown bottom topography (Dieckmann et al., 2007) and thus might have missed paths of bottom water or meanders almost parallel to the slope.

The horizontal tracer distribution in the WSBW layer at the ISPOL site (Fig. 6) shows an incoherent structure, which indicates that a single point-like source is unlikely. The patchiness might also be related to sporadic processes instead of a steady supply of newly formed waters. Additionally, the interaction of tides with small topographic features may further amplify small-scale flow features. Hence, we cannot expect to observe a synoptic field representing the spread of recently formed water masses. Instead we likely detected actual plumes or remnants of plumes and filaments in different stages, exchanging properties with the adjacent water. Enhanced ^{4}He and Ne values in the southeastern part of the ISPOL area, which are not connected to a corresponding pattern further to the west, might be caused by the intermittent discharge. However, this tongue of ^{4}He and Ne rich and low saline water could also be a permanent feature, i.e., the northern extent of an outflow from a possible canyon further south, since it is also evident in the salinity distribution of ISW-1 (Absy et al., 2008).

The estimate of glacial melt water fractions in WSBW derived with an Optimum Multiparameter Analysis (OMP) is based on hydrographic and noble gas observations. The derived glacial melt water fractions are small but significant (mean of 0.1% in WSBW, partly up to 0.4%, Fig. 8). These fractions are comparable with melt water fractions in the south, i.e. the Filchner-Ronne Ice Shelf (up to 0.5% directly in the Filchner Depression, Schlosser et al., 1990). The derived melt water fractions are strongly correlated to the ^{4}He and Ne values. For our study we rely on the values in pure glacial melt water given by Hohmann et al., (2002) (Δ^{4}He = 1060% and Δ Ne = 770%). Since reported noble gas concentrations in meteoric ice cover a wide range (see also Schlosser et al., 1990; Jean-Baptiste et al., 2001), helium isotope and neon concentrations in pure glacial melt water are still worth reconsidering.

The intermediate salinity minimum observed in upper WSBW at the ISPOL site is still apparent but weak about 700 km downstream along the Joinville section for on-slope stations. During the northward flow WSBW gains heat (+0.5°C) and the initially high noble gas content is diluted by mixing with WSDW. The off-slope WSBW does not show a salinity minimum. Its origin is associated with the Filchner Depression outflow, which reaches the bottom of the deep basin and gains even more heat (+1°C) from mixing with WSDW on its longer route.

The CFC-derived bottom water velocities and transport rates from the western slope across the Joinville (JV) section are small compared to previous reports. However, our results are based on CFC concentration ages, which account for a long-term mean tracer transport. Furthermore, mixing of newly formed WSBW with upper layers (WSDW) dilutes the CFC (and noble gas) signal. We inferred from the reduction of the noble gas concentrations between the western source and the JV section that 2/3 of initially formed WSBW is mixed upwards and does not reach the JV section colder than -0.7°C.

Combining the derived transport of WSBW and the deduced upward mixing with WSDW we find that 1.1 ± 0.5 Sv are newly formed in the western Weddell Sea by the interaction of shelf water masses with the Larsen Ice Shelf. This bottom water is shallow enough that it could leave the Weddell Basin through the gaps in the South Scotia Ridge and to supply the Antarctic Bottom Water. With a mean initial fraction of 0.10 ± 0.06 % pure glacial melt water this formation rate yields a basal melt rate of 0.35 ± 0.19 m/year or 35 ± 19 Gt/year at the base of LIS. Applying the same methods we found that 3.9 ± 1.2 Sv are formed in the southern Weddell Sea with an associated melt rate at the base of Filchner-Ronne Ice Shelf of 0.25 ± 0.11 m/year or 123 ± 53 Gt/year. These WSBW formation and basal melt rates are in very good agreement with previous findings, i.e., 4.3 ± 1.4 Sv at the FRIS, Foldvik et al (2004) and 38Gt/year at LIS and 120 Gt/year at FRIS, Hellmer (2004).

The derived WSBW composition, the formation rates, and basal melt rates bear large uncertainties due to the uncertainties in the derived source water fractions, in the transit times (due to uncertainties in the apparent CFC saturations of the source waters), and in the the mixing with the overlaying deep water. Nevertheless, they provide a complementary and independent estimate of WSBW formation and basal melt rates for the western Weddell Sea, which are in good agreement with previous estimates. In addition, they indicate consistently that the western Weddell Sea is an additional source for WSBW with the Larsen Ice Shelf directly involved in bottom water formation. It is speculative that the loss of 5000 km^2 or 5% of the total Larsen Ice Shelf (Shepherd et al., 2003) would imply a reduction of bottom water formation in the western Weddell Sea. It is even more feasible that a larger ice shelf free area, which allows more sea ice to grow and HSSW and, subsequent, WSBW to form, could compensate the glacial melt water induced WSBW formation.

Further investigations in the western Weddell Sea are necessary to confirm the findings to date and to investigate the temporal evolution. So far, we have strong indications for HSSW and glacial melt water to originate from the western Weddell Sea continental shelf, including Larsen C Ice Shelf. The spatial structure of the flow and its temporal variability just starts to become known. Bathymetric maps more reliable than those available for this area to date would be extremely helpful to interpret the results and to plan further surveys. Previous cruises to the east of the Antarctic Peninsula (in the area of Larsen Ice Shelf, i.e., ISW-1 and ISPOL) drifted within the Weddell Gyre's western rim, parallel to the slope. Hydrographic and tracer sections perpendicular to the mean flow, covering the continental shelf and slope, are desirable. They could provide a better estimate on local WSBW formation and on the relation between glacial melt water and HSSW driven processes. Furthermore, these measurements have to be related to the observed temporal changes of bottom water characteristics in the northwestern Weddell Sea (Robertson et al., 2002, Schröder et al., 2002, Nicholls et al., 2004b, Fahrbach et al., 2004). Hydropgraphic and tracer observations are always snapshots in time and space and can usually not be conducted directly at the sources in this hardly accessible and remote area. They might be complemented by model simulations that are validated by the available hydrographic and tracer observations, including those of the present study. They could also improve our understanding of the complex interaction of temporally open or sea ice covered continental shelves, the ice shelves, and the ocean interior.

Acknowledgement

We thank the master and the crew of RV Polarstern, the helicopter team, and the ISPOL scientific party for excellent and fruitful cooperation. Special thanks to Klaus Bulsiewicz, Gerd Fraas, Wilfried Plep, Jürgen Sültenfuß, and their student assistants for their excellent work in our CFC and noble gas lab. Further thanks to Andreas Wisotzki for analysis and assessment of the hydrographic data obtained during ISPOL and to Klaus-Peter Lieckfeldt and Michael Schodlok for their assistance during the noble gas and CFC sampling. We also like to thank K. Heywood and one anonymous reviewer for their helpful comments and suggestions. The tracer measurements and the data analysis carried out by O. Huhn were funded by the Deutsche Forschungsgemeinschaft (DFG), within the Schwerpunktprogramm Antarktisforschung (SPP 1158).

References

Absy, J.M., M. Schröder, R. Muench, H.H. Hellmer (2008). Early summer thermohaline characteristics and mixing in the western Weddell Sea. Deep-Sea Research II.

Beining, P., W. Roether (1996). Temporal evolution of CFC 11 and CFC 12 concentrations in the ocean interior. Journal of Geophysical Research, Vol. 101 (C7), 16455-16464.

Bullister, J.L. (1989). Chlorofluorocarbons as time-dependent tracers in the ocean. Oceanography, Vol. 2 (2), 12-17.

Bulsiewicz, K., H. Rose, O. Klatt, A. Putzka, W. Roether (1998). A capillary-column chromatographic system for efficient chlorofluoromethane measurement in ocean waters. Journal of Geophysical Research, Vol. 103 (C8), 15959-15970.

Carmack, E.D., T.D. Foster (1975). On the flow of water out of the Weddell Sea. Deep-Sea Research, Vol. 22, 711-724.

Dieckmann, G., C. Haas, M. Schröder (2007). The expeditions ANTARKTIS-XXII/1 and XXII/2 of the research Vessel "Polarstern" in 2004/2005. In *Reports on Polar Research*, Vol. 551, 37-259; edited by S. El Naggar, G. Diekmann, C. Haas, M. Schröder, M. Spindler. AWI, Bremerhaven, Germany, 37-259.

Fahrbach, E., G. Rohardt, N. Scheele, M. Schröder, V. Strass (1995). Formation and discharge of deep and bottom water in the northwestern Weddell Sea. Journal of Marine Research, Vol. 53, 515-538.

Fahrbach, E., S. Harms, G. Rohardt, M. Schröder, R.A. Woodgate (2001). Flow of bottom water in the northwestern Weddell Sea. Journal of Geophysical Research, Vol. 106 (C2), 2761-2778.

Fahrbach, E., M. Hoppema, G. Rohardt, M. Schröder, A. Wisotzki (2004). Decadal-scale variations of water mass properties in the deep Weddell Sea. Ocean Dynamics, 54, 77-91, doi. 10.1007/s10236-003-0082-3.

Foldvik, A., T. Gammelsrød, and T. Tørresen (1985). Circulation and water masses on the southern Weddell Sea shelf. In *Oceanology of the Antarctic Continental Shelf*, Antarctic Research Series, Vol. 43, 5-20.

Foldvik, A., T. Gammelsrød, E. Nygaard, S. Østerhus (2001). Current measurements near Ronne Ice Shelf: Implications for circulation and melting. Journal of Geophysical Research, Vol. 106 (C3), 4463-4477.

Foldvik, A., T. Gammelsrød, S. Østerhus, E. Fahrbach, G. Rohardt, M. Schröder, K.W. Nicholls, L. Padman, R.A. Woodgate (2004). Ice Shelf Water overflow and bottom water

formation in the southern Weddell Sea. Journal of Geophysical Research, Vol. 109, C02015, doi. 10.1029/2003JC002008.

Foster, T. D., E. C. Carmack (1976). Frontal zone mixing and Antarctic Bottom Water formation in the southern Weddell Sea. Deep-Sea Research, Vol. 23, 301-317.

Gammelsrød, T., A. Foldvik, O.A. Nøst, Ø. Skagset, L. G. Anderson, E. Fogelqvist, T. Tanhua, E.P. Jones, S. Østerhus (1994). Distribution of water masses on the continental shelf in the southern WeddellSea. In *The Polar Oceans and their role in shaping the Global Environment*, edited by O.M. Johannessen, R.D. Muench, J.E. Overland, 159-176, AGU, Washington, D.C.

Gordon, A.L., B.A. Huber, H.H. Hellmer, A. Ffield (1993). Deep and bottom water of the Weddell Sea's western rim. Science, Vol. 262, 95-97.

Gordon, A. L. (1998). Western Weddell Sea thermohaline stratification. In *Ocean, ice, and atmosphere: Interactions at the Antarctic Continental Margin*, Eds. S.S. Jacobs and R.F. Weiss; Antarctic Research Series, 75, 215-240, American Geophysical Union, Washington, D.C.

Hellmer, H.H. (2004). Impact of Antarctic ice shelf basal melting on sea ice and deep ocean properties. Geophysical Research Letters, Vol. 31, L10307, doi. 10.1029/2004GL019506.

Hellmer, H.H., C. Haas, G.S. Dieckmann, M. Schröder (2006). Sea ice feedbacks observed in the western Weddell Sea. EOS, Vol. 87 (18).

Hellmer, H.H., Ch. Haas, G. Dieckmann, M. Schröder, M. Spindler (2008). The Ice Station POLarstern (ISPOL) experiment. Deep-Sea Research II.

Hinrichsen, H., M. Tomczak (1993). Optimum Multiparameter Analysis of the water mass structure in the western North Atlantic Ocean. Journal of Geophysical Research, Vol. 98, 10155-10169.

Hohmann, R., P. Schlosser, S. Jacobs, A. Ludin, R. Weppernig (2002). Excess helium and neon in the southeast Pacific. Tracers for glacial meltwater. Journal of Geophysical Research, Vol. 107 (C11), doi. 10.1029/2000JC000378.

Hoppema, M., O. Klatt, W. Roether, E. Fahrbach, K. Bulsiewicz, C. Rodehacke, G. Rohardt (2001). Prominent renewal of Weddell Sea Deep Water from a remote source. Journal of Marine Research, Vol. 59, 257-279.

Huhn, O., W. Roether, P. Beining, H. Rose (2001). Validity limits of carbon tetrachloride as an ocean tracer. Deep-Sea Research I, Vol. 48, 2025-2049.

Jean-Baptiste, Ph., J.R. Petit, V.Y. Lipenkov, D. Raynaud, N. Barkov (2001). Constraints of hydrothermal processes and water exchange in Lake Vostok from helium isotopes. Nature, Vol. 411, 460-462.

Joughin, I., L. Padman (2003). Melting and freezing beneath Filchner-Ronne Ice Shelf, Antarctica. Geophysical Research Letters, Vol. 90 (C9), 1477, doi. 10.1029/2003GL016941.

Karstensen, J., M. Tomczak (1998). Age determination of mixed water masses with CFC and oxygen data. Journal of Geophysical Research, Vol. 103 (C9), 18599-18610

Mensch, M., W.M. Smethie, P. Schlosser, R. Wepperig, R. Bayer (1998). Transient tracer observations from the western Weddell Sea during the drift and recovery of Ice Station Weddell. In *Ocean, ice, and atmosphere: Interactions at the Antarctic Continental Margin*, Eds. S.S. Jacobs and R.F. Weiss; Antarctic Research Series, 75, 241-256, American Geophysical Union, Washington, D.C.

Millero, F. J. (1978). Annex 6, freezing point of seawater. Unesco Technical Papers in the Marine Sciences, 28, 29-35.

Nicholls, K.W., L. Padman, M. Schröder, R.A. Woodgate, A. Jenkins, S. Østlund (2003). Water mass modification over the continental shelf north of Ronne Ice Shelf, Antarctica. Journal of Geophysical Research, Vol. 108 (C8), 3260, doi. 10.1029/2002JC001713.

Nicholls, K.W., S. Østerhus (2004a). Interannual variability and ventilation timescales in the ocean cavity beneath Filchner-Ronne Ice Shelf, Antarctica. Journal of Geophysical Research, Vol. 109, C04014, doi. 10.1029/2003JC002149.

Nicholls, K.W., C.J. Pudsey, P. Morris (2004b). Summertime water masses off the northern Larsen C Ice Shelf, Antarctica. Geophysical Research Letters, Vol. 31, L09309, doi. 10.1019./2004GL019924.

Orsi, A.H., G.C. Johnson, J.L. Bullister (1999). Circulation, mixing and production of Antarctic Bottom Water. Progress in Oceanography, Vol. 43, 55-109.

Prinn, R. G., R. F. Weiss, P. J. Fraser, P. G. Simmonds, D. M. Cunnold, F. N. Alyea, S. O'Doherty, P. Salameh, B. R. Miller, J. Huang, R. H. J. Wang, D. E. Hartley, C. Harth, L. P. Steele, G. Sturrock, P. M. Midgley, A. McCulloch (2000). A history of chemically and radiatively important gases in air deduced from ALE/GAGE/AGAGE. Journal of Geophysical Research, Vol. 105, 17.751-17.792.

Robertson, R., M. Visbeck, A.L. Gordon, E. Fahrbach (2002). Long-term temperature trends in deep waters of the Weddell Sea. Deep-Sea Research II, Vol. 49, 4791-4806.

Rodehacke, C.B., H.H. Hellmer, O. Huhn, A. Beckmann (2006). Ocean/ice shelf interaction in the southern Weddell Sea. Results of a regional numerical helium/neon simulation. Ocean Dynamics, doi. 10.1007/s10236-006-0073-2.

Roether, W., R. Well, A. Putzka, C. Rüth (1998). Component separation of oceanic helium. Journal of Geophysical Research, Vol. 103 (C12), 27931-27946.

Roether, W., R. Well, A. Putzka, C. Rüth (2001). Corrections to "component separation of oceanic helium". Journal of Geophysical Research, Vol. 106 (C3), 4679.

Schlosser, P. (1986). Helium. A new tracer in Antarctic oceanography. Nature, Vol. 321, 233-235.

Schlosser, P., R. Bayer, A. Foldvik, T. Gammelsrød, G. Rohardt, K.O. Münnich (1990). Oxygen 18 and helium as tracers of Ice Shelf Water and winter/ice interaction in the Weddell Sea. Journal of Geophysical Research, Vol. 95 (C3), 3253-3263.

Schodlok, M., H.H. Hellmer, A. Beckmann (2002). On the transport, variability and origin of dense water masses crossing the South Scotia Ridge. Deep-Sea Research II, Vol. 49 (21), 4807-4825.

Schröder, M, H.H. Hellmer, J.M. Absy (2002). On the near-bottom variability in the northwestern Weddell Sea. Deep-Sea Research II, Vol. 49, 4767-4790.

Shepherd, A., D. Wingham, T. Payne, P. Skvarca (2003). Larsen Ice Shelf has progressively thinned. Science, Vol. 302, 856-859.

Sonnerup, R.E. (2001). On the relations among CFC derived water mass ages. Geophysical Research Letters, Vol. 28 (9), 1739-1742.

Sültenfuß, J., M. Rhein, W. Roether (2007). The Bremen Mass Spectrometric Facility for the measurement of helium isotopes, neon, and tritium in water. International Symposium on Quality Assurance for Analytical Methods in Isotope Hydrology, IAEA Proceedings, IAEA-CN 119-7, in press.

Tomczak, M. (1981). A multi-parameter extension of temperature/salinity diagram techniques for the analysis of non-isopycnal mixing. Progress in Oceanography, Vol. 10, 147-171.

Tomczak, M., D.G.B. Large (1989). Optimum Multiparameter Analysis of mixing in the thermocline of the Eastern Indian Ocean. Journal of Geophysical Research, Vol. 94 (C11), 16141-16149.

Walker, S.J., R.F. Weiss, P.K. Salameh (2000). Reconstructed histories of the annual mean atmospheric mole fractions for the halocarbons CFC-11, CFC-12, CFC-113 and carbon tetrachloride. Journal of Geophysical Research, Vol. 105, 14285-14296.

Warner, M.J., R.F. Weiss (1985). Solubilities of chlorofluorocarbons 11 and 12 in water and seawater. Deep-Sea Research, Vol. 32, 1485-1497.

Waugh, D.W., T.M. Hall, T.W.N. Haine (2003). Relationships among tracer ages. Journal of Geophysical Research, Vol. 108 (C5), doi. 10.1029/2002JC001325.

Well, R., J. Lupton, W. Roether (2001). Crustial helium in deep Pacific waters. Journal of Geophysical Research, Vol. 106 (C7), 14165-14177.

Well, R., W. Roether (2003). Neon distribution in South Atlantic and South Pacific waters. Deep-Sea Research I, Vol. 50, doi. 10.1016/S0967-0637(03)00058-X, 721-735.

Well, R., W. Roether, D.P. Stevens (2003). An additional deep water mass in Drake Passage as revealed by ^{3}He data. Deep-Sea Research I, Vol. 50, 1079-1098, doi. 10.1016/S0967-0637(03)00050-5.

Weppernig, R., P. Schlosser, S. Khatiwala, R.G. Fairbanks (1996). Isotope data from Ice Station Weddell: Implications for deep water formation in the Weddell Sea. Journal of Geophysical Research, Vol. 101 (C10), 25723-25739.

Weiss., R.F. (1971). Solubility of helium and neon in water and seawater. Journal of Chemical Engineering Data, Vol. 16, 235-241.

Weiss, R.F., H.G. Østlund, H. Craig (1979). Geochemical studies of the Weddell Sea. Deep Sea Research, Part A, Vol. 26, 1093-1120.

Weiss, R.F., J.L. Bullister, R.H. Gammon, M.J. Warner (1985). Atmospheric chlorofluoromethanes in the deep equatorial Atlantic. Nature, Vol. 314, 608-610.

TABLES

Table 1

	Δ^4He	δ^3He	ΔNe
ANT XII/3	+0.5%	-0.4%	-0.1%
ANT XIII/4	+0.4%	-0.6%	+0.1%
ANT XV/4	+0.8%	-0.3%	+0.3%
ISPOL	-0.6%	-0.0%	-1.9%

Table 1: Adjustment of He isotope and Ne measurements relative to archived data sets (e.g. CCHDO archive).

Table 2

	WW[1]	WDW[1]	HSSW[2]	glacial melt water[3]	ISW[4]
limits	$\theta < -1.80$°C $\sigma_1 < 32.46$ depth > 30 m	$\theta > 0$°C $\sigma_1 > 32.5$	$\theta < -1.80$ $\sigma_1 > 32.71$ (S > 34.70)		$\theta < T_f$
θ [°C]	-1.84 ± 0.01	0.35 ± 0.15	-1.93 ± 0.02	-2.3 ±0.3	-2.15 ±0.05
S	34.38 ± 0.02	34.67 ± 0.01	34.82 ± 0.05	0.00 ± 0.00	34.64 ± 0.04
^{4}He [nmol/kg]	1.86 ± 0.02	1.88 ± 0.02	1.92 ± 0.01	25.7 ± 2.6	2.14 ± 0.04
Ne [nmol/kg]	8.22 ± 0.07	8.13 ± 0.06	8.47 ± 0.04	89.2 ± 9.0	9.19 ± 0.1
δ^3He [%]	-0.11 ± 0.25	7.15 ± 0.63	-0.81 ± 0.21	-2.00 ± 0.5	-1.80 ± 0.10
CFC-11 [ppt]	2004: 171 ± 5	2004: 36 ± 12	1995: 157 ± 15	0.0 ± 0.0	no data
(S_{CFC-11} [%])	(68 ± 2)	(14 ± 4)	(60 ± 5)		
CFC-12 [ppt]	2004: 380 ± 5	2004: 78 ± 24	1995: 302 ± 27	0.0 ± 0.0	no data
(S_{CFC-12} [%])	(70 ± 2)	(14 ± 4)	(60 ± 5)		

Table 2: Definition limits, means, and errors (standard deviations) as characteristic values and uncertainties of source water masses used for the OMP analysis

[1]Defined in the western Weddell Sea, i.e., ISPOL (ANTXXII/2) data.

[2]Defined in the southwestern Weddell Sea (ANT XII/3, subsection c). CFC data refer to 1995. Saturations S are also based on t_{obs} = 1995 and Δt = 0 years (Eq. 2). Accounting for a residence time Δt = 5 years for HSSW (Mensch et al., 1998; Nicholls et al., 2004a), the apparent saturation becomes 63%, and for a transit time Δt = 3 years the apparent saturation becomes 61% (see text).

[3]The temperature was calculated after Millero (1978) for S = 0 and an assumed ice shelf draft of 500 dbar. [4]He and Ne are from Hohmann et al. (2002), who used measured air content in ice cores and the atmospheric partial pressures of these gases. The error reflects roughly half of the variation of the air measurements from different drilling sites. The δ^3He value assumes a constant atmospheric isotope ratio trapped in the ice matrix (unpublished results from Sültenfuß, pers. com., 2006, indicate much smaller δ^3He values in gas samples from ice cores, presumably due to fractionation, since the lighter ^{3}He isotope might escape more easily from the ice matrix).

[4]Within Filchner Depression (from Schlosser et al., 1990). The ISW characteristics are included just for completeness. The value for Ne is estimated from the helium value and the atmospheric He/Ne ratio.

Table 3

	θ	S	^{4}He	Ne	δ^3He
WW	-0.78	-0.70	-0.23	+0.03	-0.79
WDW	+0.99	+0.68	-0.33	-0.59	+0.98
HSSW	-0.90	-0.49	+0.67	+0.85	-0.88
melt water	-0.24	-0.20	+0.95	+0.89	-0.21

Table 3: Correlation coefficients between OMP derived source water mass fractions and observed properties in the analyzed deep and bottom waters. The signs indicate weather the properties are correlated or anti-correlated.

Table 4

	S_{WW}	S_{WDW}	S_{HSSW}
CFC-11 (western source for on-slope)	68 ± 2 %	14 ± 4 %	61 ± 5 % [1]
CFC-12 (western source for on-slope)	70 ± 2 %	14 ± 4 %	61 ± 5 % [1]
CFC-11 (southern source for off-slope)	65 ± 6 %	9 ± 5%	63 ± 6 % [2]
CFC-12 (southern source for off-slope)	66 ± 5 %	10 ± 7%	64 ± 6 % [2]

Table 4. Apparent CFC saturations S in source water masses; for "on-slope" WSBW derived from CFC observations in the western Weddell Sea (ISPOL) and for "off-slope" WSBW derived from observations in the southern Weddell Sea (ANT XII/3).

[1]accounting for an additional transit time $\Delta t = 3$ years (Eq. 2)

[2]accounting for a residence time of 5 years (Eq. 2) within the ice shelf cavity before re-entering the circulation and becoming involved in bottom water formation (Mensch et al., 1998; Nicholls et al., 2004a)

FIGURES

Figure 1A

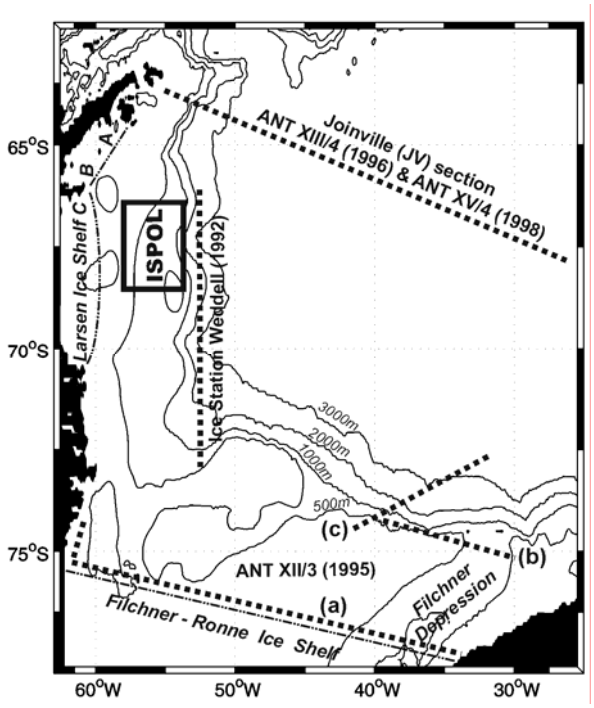

Figure 1B

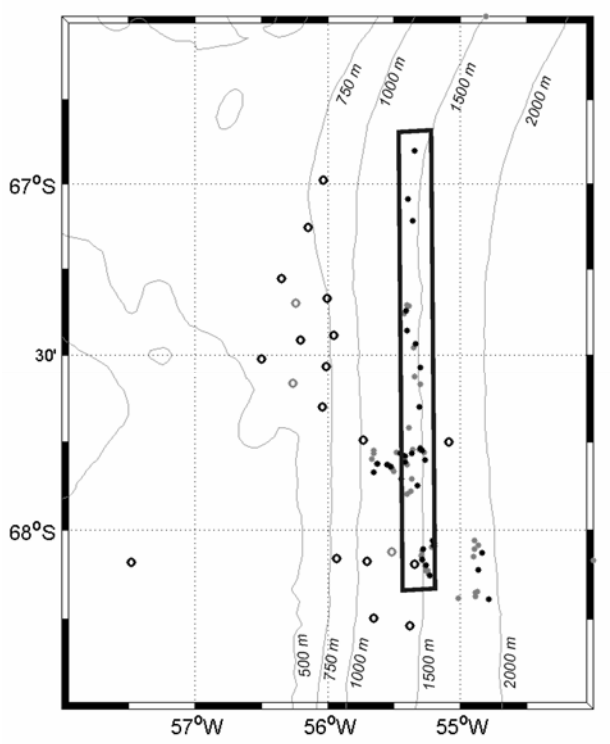

Fig. 1. Map (A) sketches the western Weddell Sea with hydrographic and tracer sections used in this paper. The location of the ISPOL site as shown in map (B) is indicated by the rectangle in the upper left. Small letters a, b, and c indicate subsections of cruise ANT XII/3. Geographical features are named in italic letters. Capital letters A, B, and C denote parts of the Larsen Ice Shelf. The dash-dotted lines indicate the ice shelf edges. Map (B) of ISPOL stations (dots = ship stations, open circles = helicopter stations; stations with available tracer measurements are highlighted bold; the rectangle marks stations used for vertical section in Fig. 4). Thin grey lines indicate isobaths. Note that water depths observed during ISPOL differed widely from the available bathymetric maps, in the northwestern part CTD profiles were more than 200 m shallower and in the southeastern part 50 m deeper. Compare also Fig. 4, and Dieckmann et al. (2007).

Figure 2

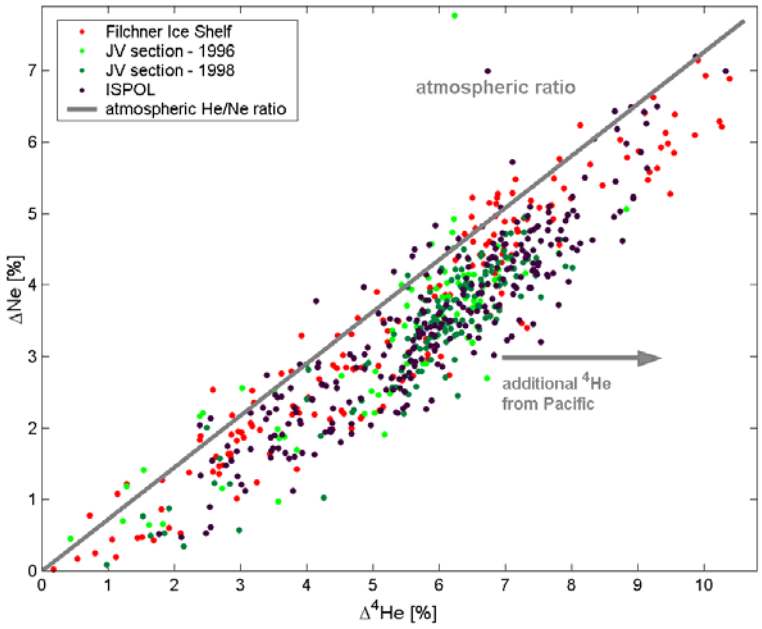

Fig. 2: Δ^4He vs. ΔNe from various cruises in the Weddell Sea. Red dots = ANT XII/2 (1995), light green = ANT XIII/4 (1996), dark green = ANT XV/4 (1998), black = ANT XXII/2 (ISPOL, 2004) corrected with Δ^4He -0.6% and ΔNe -1.9%. The grey line represents the addition of atmospheric air with constant ^{4}He/Ne ratio (e.g. from bubble injection from atmosphere or melted glacial ice). The grey arrow indicates ^{4}He addition from Pacific water (CDW) particularly in the WDW layer.

Figure 3

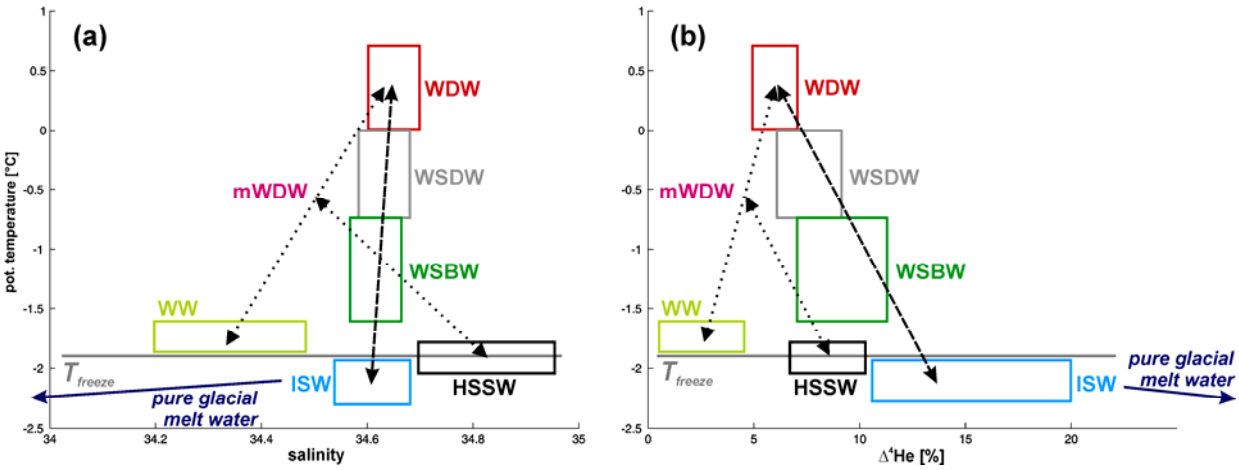

Fig. 3. Mixing scheme for WSBW formation in (a) θ (potential temperature) and S (salinity) space and (b) in θ and Δ^4He space. Glacial melt water is indicated by the dark blue arrow pointing to its characteristic values far outside the sketch. The horizontal grey line is the surface freezing temperature. The two dotted lines represent the mixing of WDW with WW to form modified WDW (mWDW) and further mixing with HSSW (Foster-Carmack process). The dashed line represents WSBW formation by mixing of WDW with ISW or glacial melt water (Foldvik process).

Figure 4

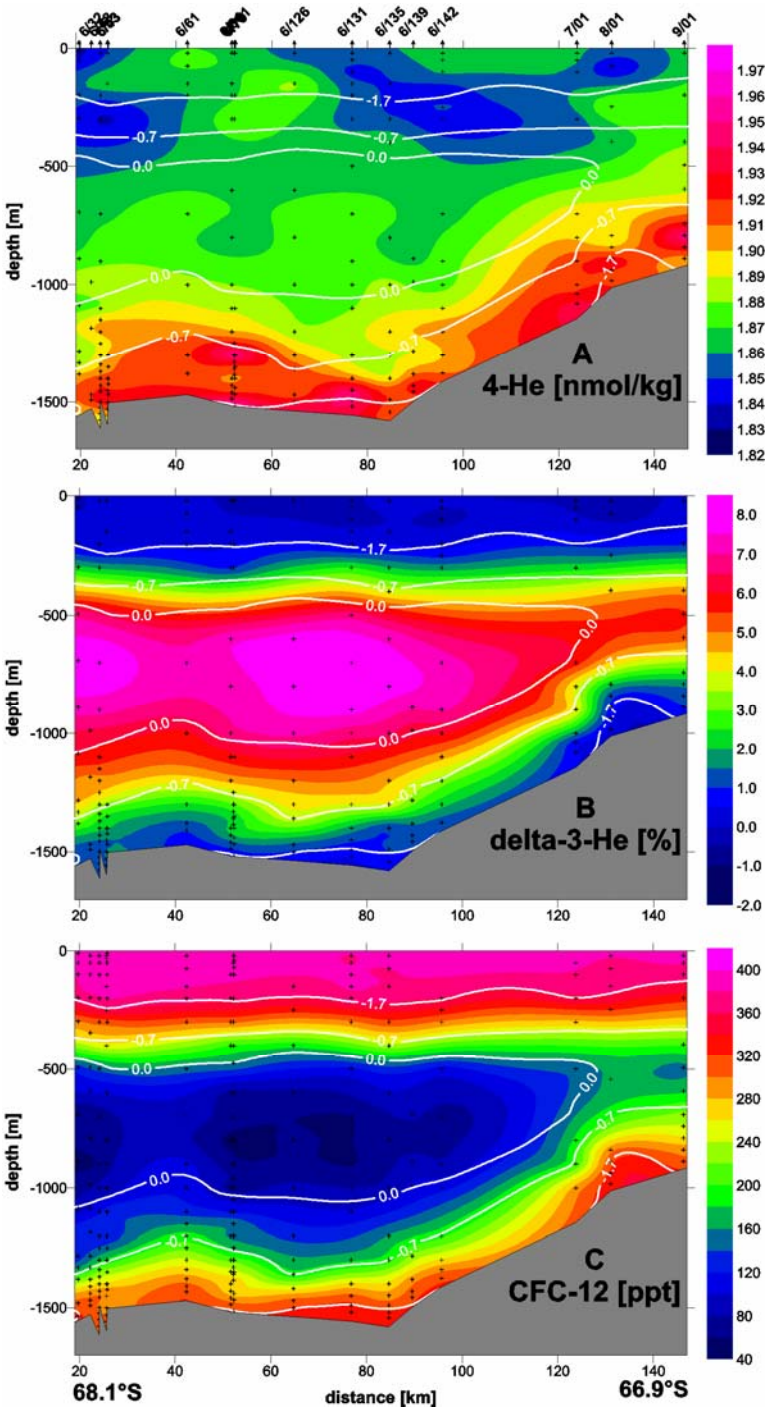

Fig. 4: Vertical sections of A: ^{4}He [nmol/kg], B: δ^{3}He [%], and C: CFC-12 [ppt]. Used are bottle data from stations with tracer measurements along the main ISPOL drift track (framed in Fig. 1B) from south (left) to north (right). Isotherms of 0°C and -0.7°C mark the transitions between WDW/WSDW and WSDW/WSBW, respectively. The deep -1.7°C isotherm is included to mark the cold bottom layer. Selected stations (station/cast labeled on top of panel A) are not all identical with those of Absy et al. (2008, Fig. 5).

Figure 5A

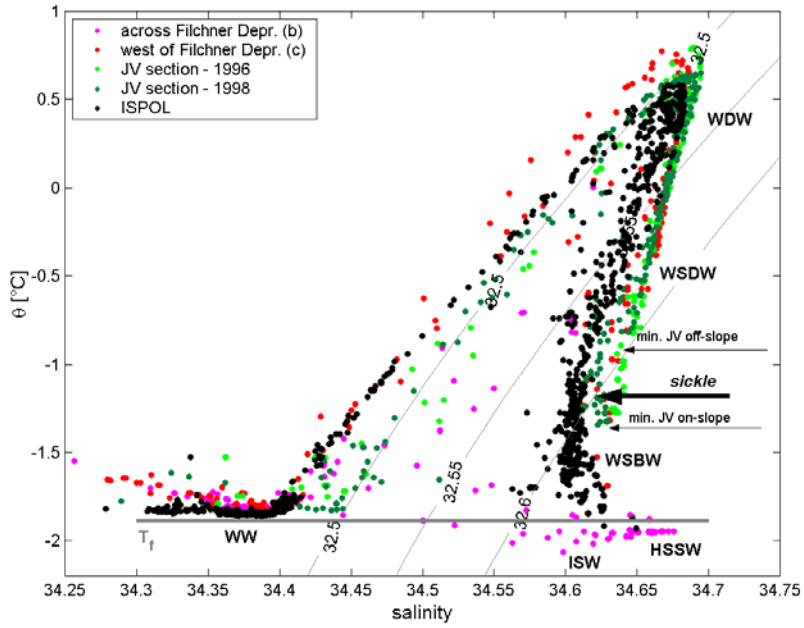

Fig. 5A. θ-S diagram of bottle data from ISPOL (ANT XXII/2, black dots). Included are observations from ANT XII/3 (sub-sections b and c) from stations north of the Filchner Depression (pink) and west of it (red), and from ANT XIII/4 (light green) and ANT XV/4 (dark green) from stations west of 45°W (see Fig. 1). Isopycnals σ_1 = 32.50, 32.55, and 32.60, and surface freezing temperature (T_f) are indicated by thin lines. Thick arrow indicates the sickle-shaped salinity minimum. Thin arrows mark minimum temperatures on-slope and off-slope along the JV section (see text).

Figure 5B

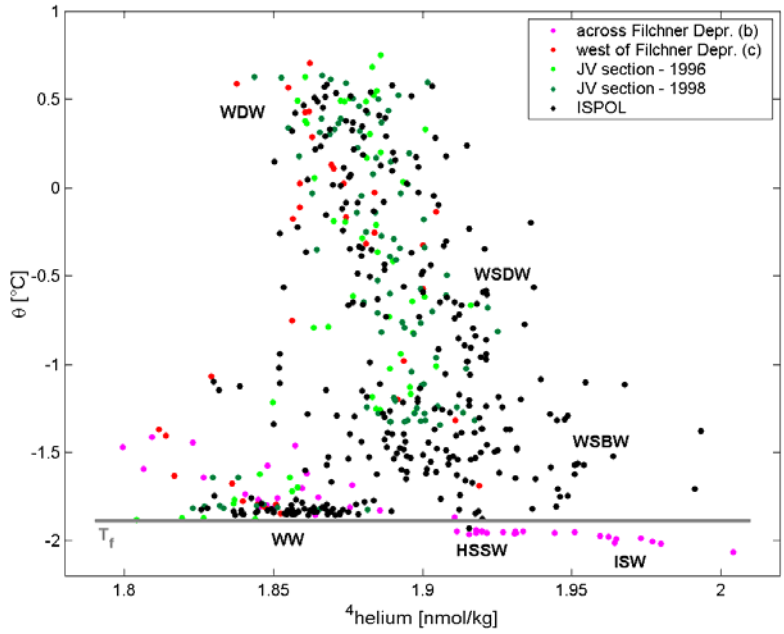

Fig. 5B. Same as Fig. 5A, but for θ vs. ^{4}He. Note that due to the data scatter the data points of the upper (from WW to WDW) and lower arm (from WDW to WSBW; cf. Fig. 5A) are not clearly separated.

Figure 5C

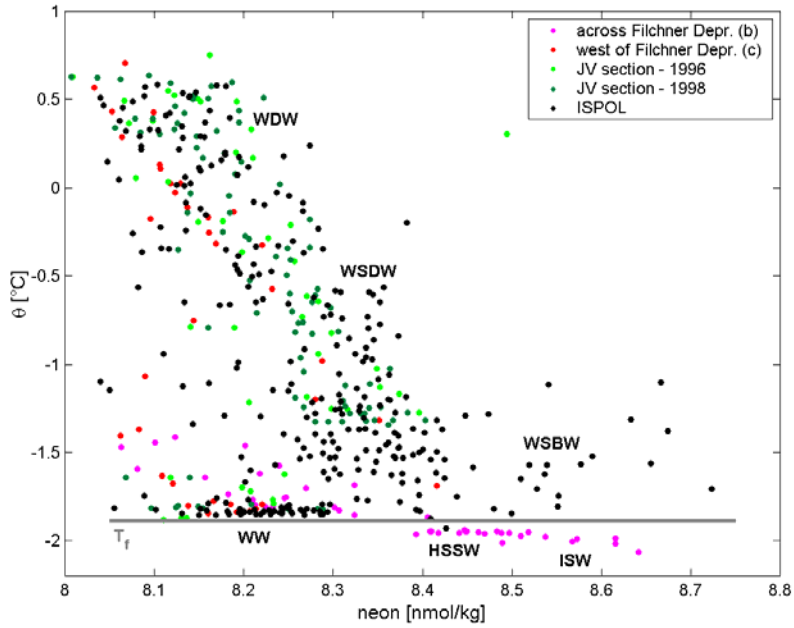

Fig. 5C. Same as Fig. 5A, but for θ vs. Ne. Data overlap between upper and lower arm as in Fig. 5B.

Figure 5D

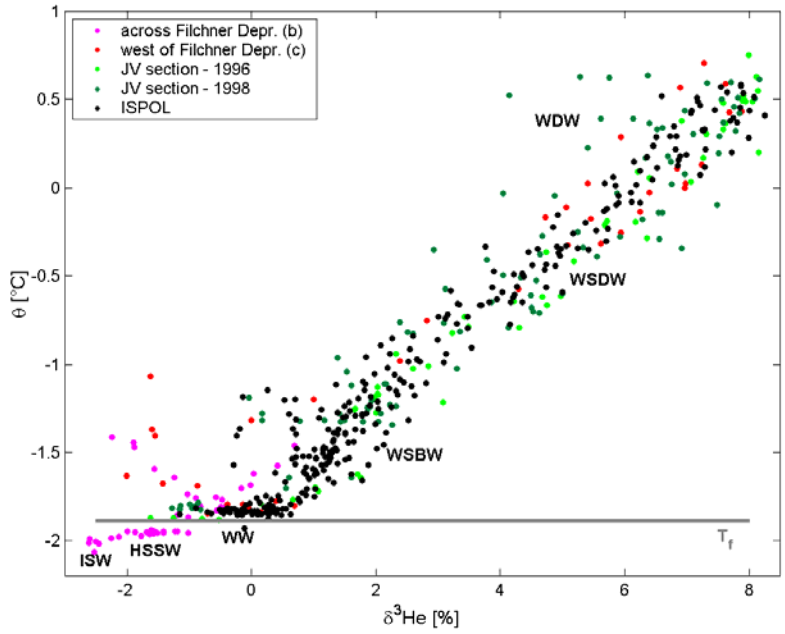

Fig. 5D. Same as Fig. 5A, but for θ vs. δ^3He. The data of the upper and lower arm (cf. Fig. 5A) fully overlap.

Figure 5E

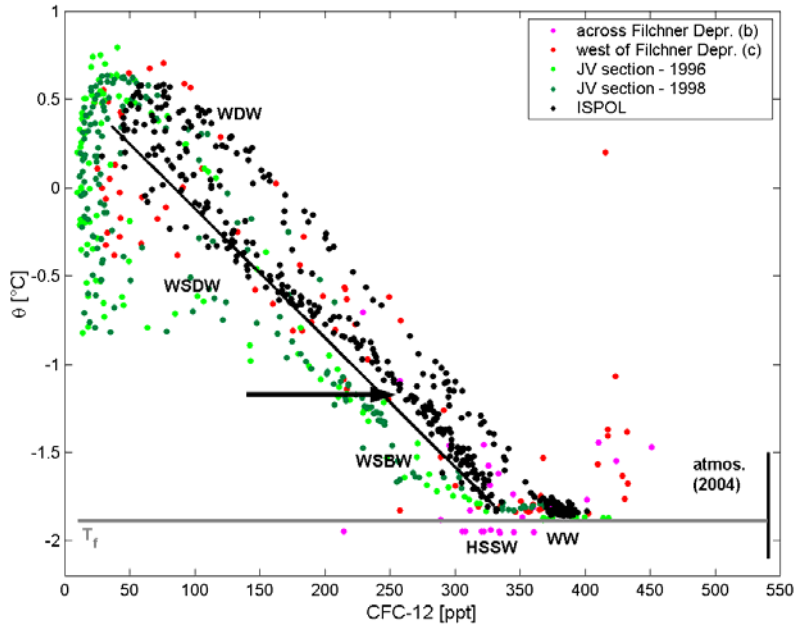

Fig. 5E. Same as Fig. 5A but for θ vs. CFC-12 [ppt] from different years. The solid line to the right marks the atmospheric partial pressure for 2004. A mixing line between the ISPOL CFC minimum and the bottom layer values is included to reveal the slightly enhanced CFC-12 values in the upper WSBW layer (thick arrow, see text).

Figure 6

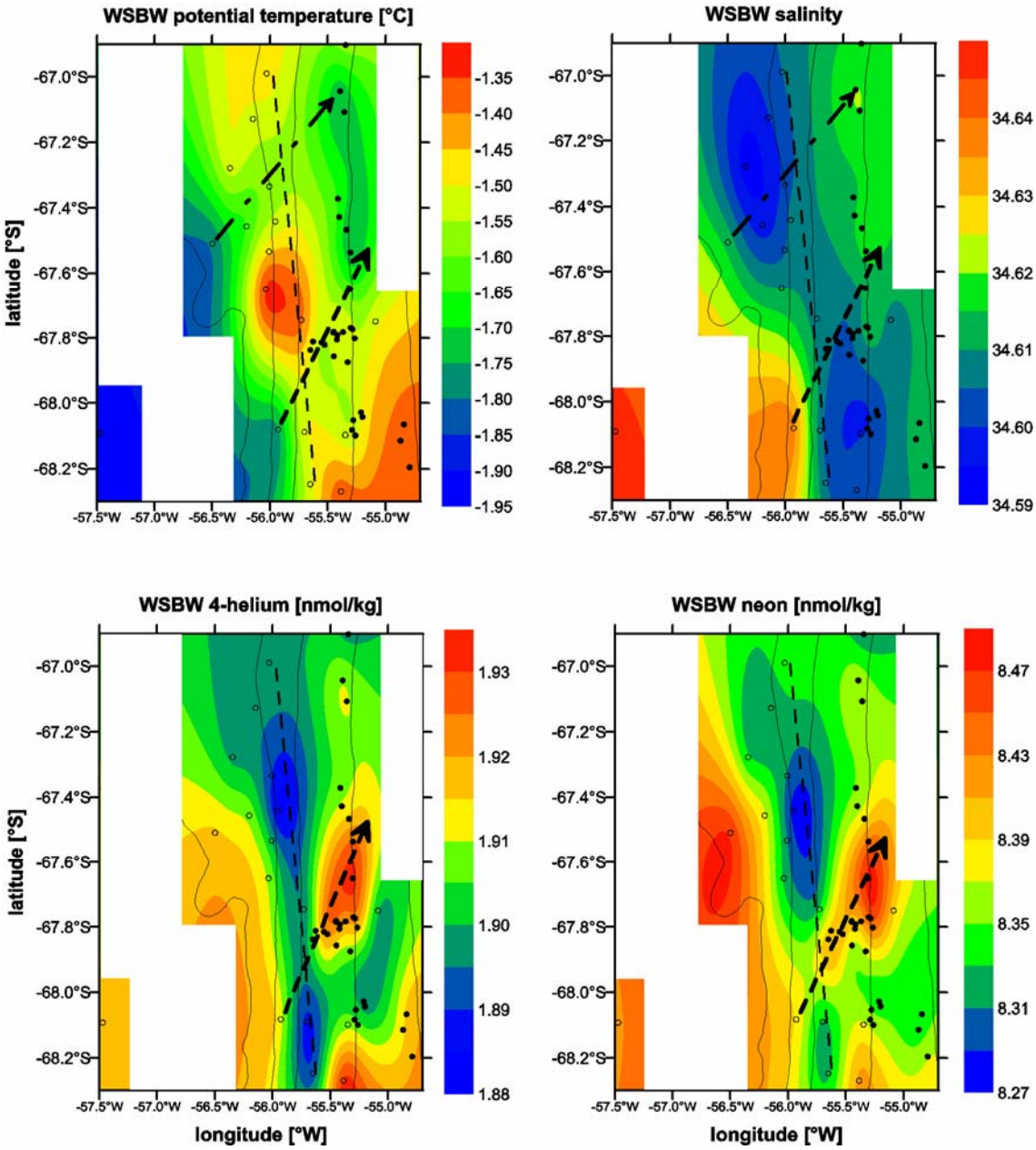

Fig. 6. Horizontal distributions of θ, S, ^{4}He and Ne in the bottom layer. Contours of neutral densities (not shown) are almost parallel to θ contours. Thin black lines indicate isobaths as in Figure 1B (water depths vary roughly between 500 m in the west and 2000 m in the east). Included are values directly at the bottom from stations with available ^{4}He and Ne (helicopter stations indicated by open circles, ship casts by dots). The spacing of the contour lines for ^{4}He and Ne corresponds to the accuracy of the measurements. Areas without data are blanked. For straight lines and arrows see text.

Figure 7

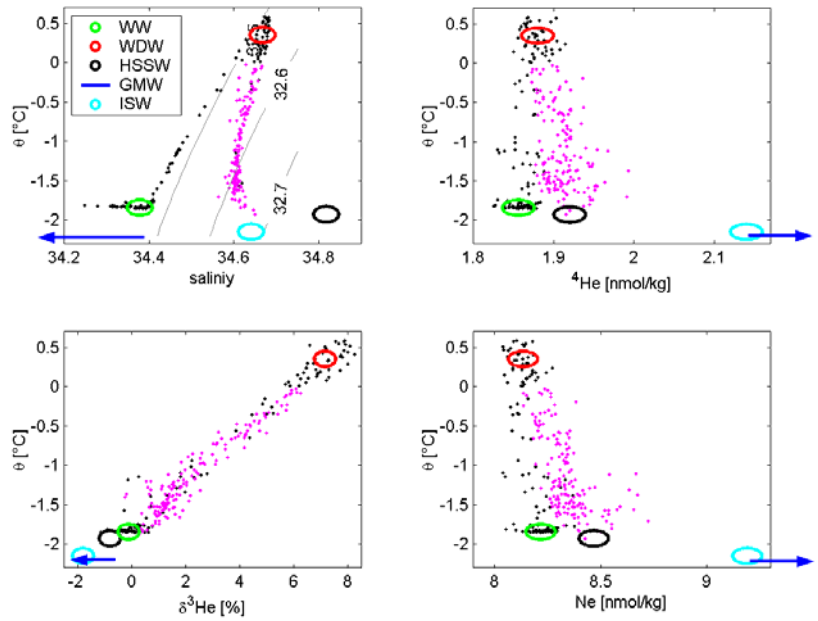

Fig. 7. Observed parameter distributions for the ISPOL cruise data. Pink dots are observations within WSDW (θ < 0°C) and WSBW (θ < -0.7°C) analyzed by the OMP. The ellipses schematically represent the characteristics of the source water masses WW (green), WDW (red), HSSW (black), and ISW (cyan) (see Table 2) with sizes proportional to the uncertainties. Note that the properties of glacial melt water lie outside the displayed range.

Figure 8

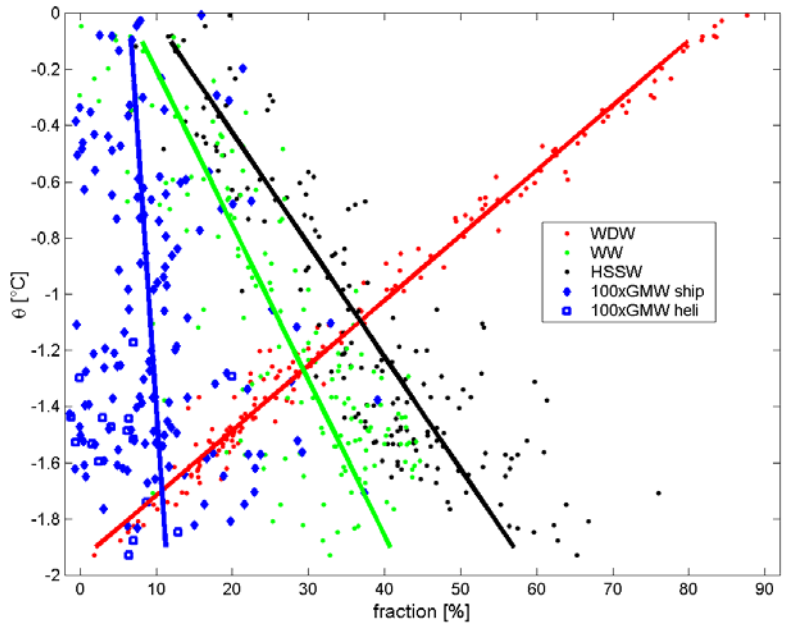

Fig. 8. Relative fractions of source water masses (WDW = red, WW = green, HSSW = black, glacial melt water = blue) within WSDW and WSBW vs. θ. Note that the glacial melt water fractions are multiplied by 100. Solid lines are linear regressions.

Figure 9

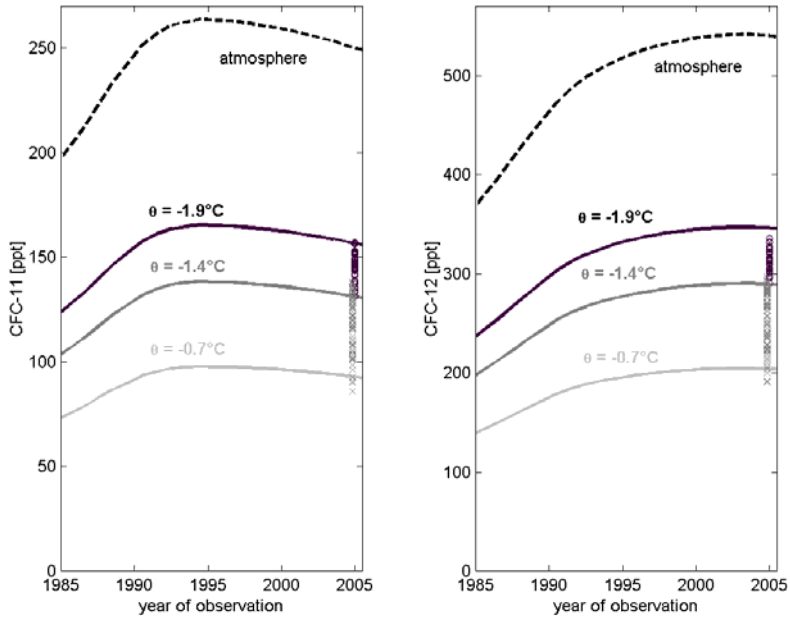

Fig. 9. CFC-11 and CFC-12 atmospheric histories (dotted lines) and reconstructed CFC histories according to Eq. 3 (black solid line for θ = -1.9°C, grey for θ = -1.4, and light grey for θ = -0.7°C). Black circles are observed CFC values within lower layers of WSBW (-1.9 < θ < -1.4°C) and grey x within upper layers of WSBW (-1.4 < θ < -0.7°C) from the ISPOL site.

Figure 10

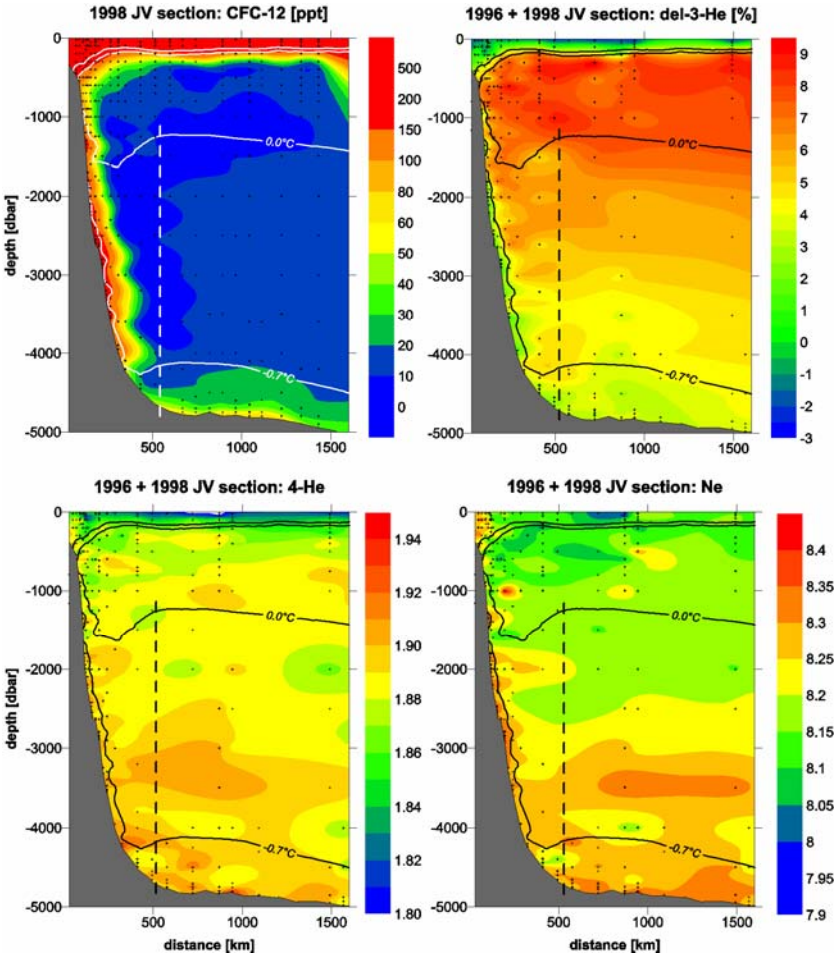

Fig. 10. Sections of CFC-12 (partial pressure [ppt]) along the JV section of 1998 (Fig. 1A), and combined JV sections of 1996 and 1998 for δ^3He, ^{4}He, and Ne. The 0°C isotherm marks the transitions between WDW and WSDW and -0.7°C between WSDW and WSBW. The vertical dashed line marks the boundary between on-slope and off-slope (see text).

Figure 11

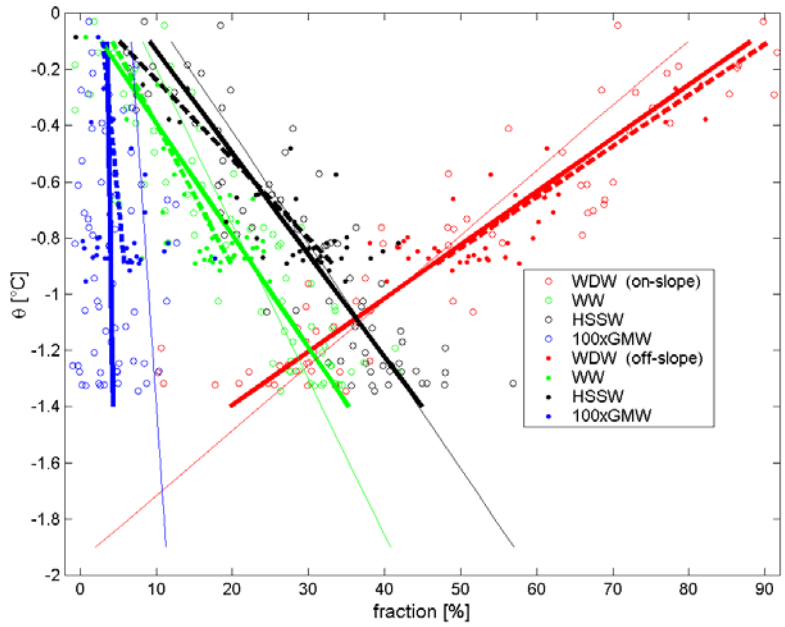

Fig. 11. Relative fractions of source water masses (WDW = red, WW = green, HSSW = black, glacial melt water = blue) within WSDW and WSBW vs. θ for JV section (analogue to Fig. 8). Note that the glacial melt water fractions were multiplied by 100. Open circles are fractions (solid lines the linear regressions) derived from observations in on-slope WSBW and dots (and dashed lines) are from off-slope WSBW. For comparison the linear regressions from the ISPOL (Fig. 8) analysis are included as thin lines.

Figure 12

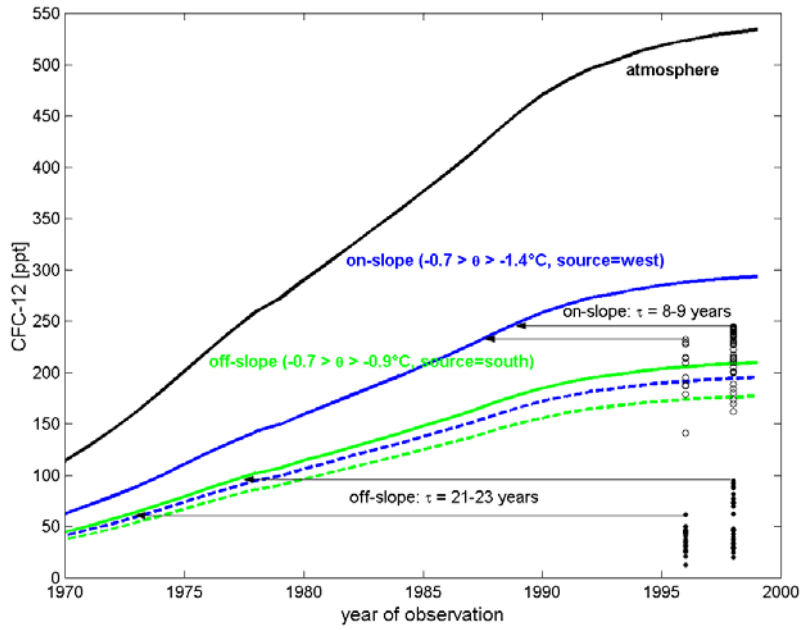

Fig. 12. CFC-12 atmospheric history (black line) and reconstructed histories according to Eq. 3. Blue lines based on source water fractions and CFC-12 saturations in on-slope WSBW, solid line for θ = -1.4°C (θ_{min} on-slope WSBW), dashed for θ = -0.7 (θ_{max} WSBW). Greene lines based on source water fractions and CFC-12 saturations for off-slope WSBW, solid line for θ = -0.9°C (θ_{min} off-slope WSBW), dashed for θ = -0.7 (θ_{max} WSBW). Open circles are CFC-12 observations within on-slope WSBW and dots are within off-slope WSBW. Arrows indicate time shift between observations and the atmospheric CFC-12 history (i.e., the transit times or CFC-12 concentration ages).

Figure 13

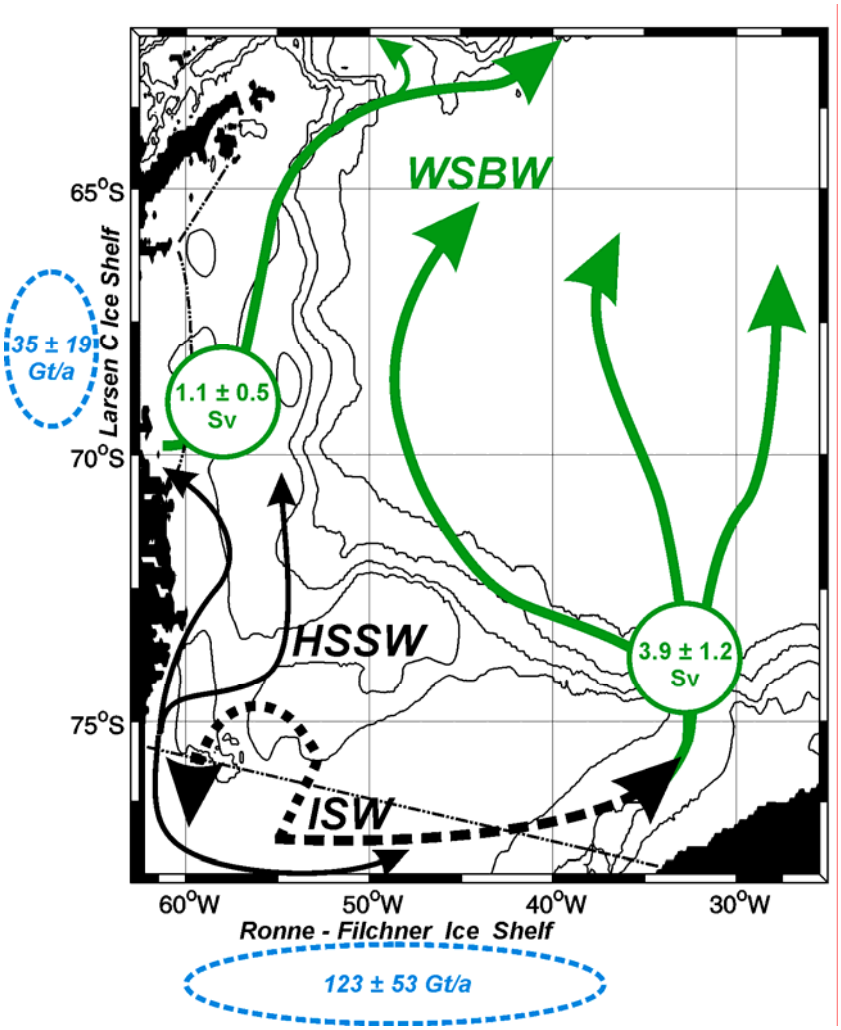

Fig. 13. Schematic of water mass spreading in the southern and western Weddell Sea. Green arrows = WSBW, thin black arrows = HSSW, and dotted black arrows = ISW. Numbers in circles denote derived WSBW formation rates (solid) and ice shelf basal melt rates (blue dotted).